

Linear viscoelasticity and time-temperature-salt and other superpositions in polyelectrolyte coacervates

Ronald G. Larson, Ying Liu and Hailing Li

Citation: *Journal of Rheology* **65**, 77 (2021); doi: 10.1122/8.0000156

View online: <https://doi.org/10.1122/8.0000156>

View Table of Contents: <https://sor.scitation.org/toc/jor/65/1>

Published by the [The Society of Rheology](#)

ARTICLES YOU MAY BE INTERESTED IN

[Determining threadlike micelle lengths from rheometry](#)

Journal of Rheology **65**, 59 (2021); <https://doi.org/10.1122/8.0000152>

[Strategy for reducing molecular ensemble size for efficient rheological modeling of commercial polymers](#)

Journal of Rheology **65**, 43 (2021); <https://doi.org/10.1122/8.0000125>

[Rheological responses of particle-filled polymer solutions: The transition to linear-nonlinear dichotomy](#)

Journal of Rheology **65**, 1 (2021); <https://doi.org/10.1122/8.0000097>

[Rheology discussions: The physics of dense suspensions](#)

Journal of Rheology **64**, 1501 (2020); <https://doi.org/10.1122/8.0000174>

[Data-driven physics-informed constitutive metamodeling of complex fluids: A multifidelity neural network \(MFNN\) framework](#)

Journal of Rheology **65**, 179 (2021); <https://doi.org/10.1122/8.0000138>

[Revisiting the basis of transient rheological material functions: Insights from recoverable strain measurements](#)

Journal of Rheology **65**, 129 (2021); <https://doi.org/10.1122/8.0000154>



The advertisement features a composite image. On the left, a young child in a blue shirt sits on a glowing red line that recedes into the distance. In the center, two Anton Paar rheometers are shown. The text 'True powder rheology' is prominently displayed in the upper right. The Anton Paar logo and name are in the bottom right corner. A 'Find out more' button is located at the bottom center.

True powder rheology

 **Anton Paar**

[Find out more](#)



Linear viscoelasticity and time-temperature-salt and other superpositions in polyelectrolyte coacervates

Ronald G. Larson,^{1,2} Ying Liu,² and Huiling Li²

¹*Department of Chemical Engineering, University of Michigan, Ann Arbor, Michigan 48109*

²*Macromolecular Science and Engineering Program, University of Michigan, Ann Arbor, Michigan 48109*

(Received 1 September 2020; final revision received 4 December 2020; published 6 January 2021)

Abstract

The linear viscoelasticity of coacervates formed by oppositely charged polyelectrolytes in the salt solution is reviewed, with a focus on time-temperature, time-salt, time-*pH*, and time-hydration superpositions, and on fundamental relaxation mechanisms. A variety of polyelectrolyte pairs are covered, showing the frequent, but not universal, success of the time-salt superposition. Master curves in many cases are similar to those for neutral polymers, including Rouse and reptation theories. However, in some cases, solidlike, as opposed to fluidlike, response is observed at low frequencies, especially at low salt concentrations. Some coacervates seem to fit “sticky diffusion” theory reasonably well, wherein relaxation is controlled by the breakage rate of ion pairs; the dependence of the “sticker” lifetime on salt concentration has been explored but is not well understood as yet. It is also possible that local relaxation is not controlled by breakage of ion pairs but by cooperative, “glassy,” relaxation of monomers, salt ions, and water molecules. Compilation and comparison of different datasets and suggested formulas for rheological time constants are presented, and some suggestions are given for future directions. © 2021 The Society of Rheology. <https://doi.org/10.1122/8.0000156>

I. INTRODUCTION

One of the last remaining fields of polymer science for which the linear rheology remains mysterious is that of coacervates formed by mixing water-soluble polyelectrolytes (PEs) of the opposite sign in the presence of salts and water. The rheology of polymer-rich phases formed by such mixtures ranges from hard solid, to soft gel, to liquid, depending on the polymer type, molecular weight, salt concentration, and other properties. While there does not appear to be a sharp boundary distinguishing “coacervates” from “precipitates,” the latter are dense, hard, mixtures of oppositely charged polymers, and are “glassy,” or nonequilibrium, whereas coacervates, also called “polyelectrolyte complexes” (or PECs), are either soft gel-like solids or viscous fluids that are at thermodynamic equilibrium or at least close to it. In this Review, we focus on coacervates, whose rheology is more readily measured than is the case for precipitates. There is a wide range of uses of these coacervates, ranging from food and personal care products to drug release compounds, underwater adhesives, and others, as reviewed recently by Liu *et al.* [1].

Despite their wide range of applications and growing interest in their structure and dynamics, physical properties, and rheology, coacervates remain mysterious. Even basic scaling laws, such as the dependence of zero-shear viscosity and relaxation time on molecular weight, and on concentrations of PEs and salts, remain uncertain. The lack of reliable quantitative theories for coacervates, analogous to the Rouse theory of unentangled neutral polymers, and the reptation theory for entangled ones, is a glaring gap. The theory that is closest to playing this role for coacervates is the “sticky diffusion” theory of associating polymers [2], which has been

applied to coacervate rheology, but with uneven success, as we will see in what follows. Reasons for the gaps in theoretical understanding include (1) the rarity of experimental studies on comprehensive series of nearly monodisperse polymers over a wide range of molecular weights; (2) the relative difficulty in controlling and measuring salt, water, and polymer concentrations in the coacervate phase because it is typically prepared by phase separation; (3) sensitivity to ion- and monomer-specific interactions, including PE charge density, monomer sequence, hydrogen bonding, chirality, π - π stacking, etc. [3], thus impeding “universal” scaling laws that transcend specific chemistry; (4) the complexity of the physical phenomena governing coacervates, which includes electrostatics, ion-binding of one PE to another of the opposite charge, binding to salt ions, entanglements, and hydrophobic interactions; (5) asymmetries between the two coacervate PEs in the effect on rheology of chain length, charge density, concentration, etc.; and (6) the large number of parameters, including the concentrations and molecular weights of each of the two PEs, concentrations and types of salt, etc. The above list does not even consider the case of charge regulation and *pH* dependencies of rheology for “weak” PEs, whose charge states are sensitive to *pH* and chemical environment.

These challenges are slowly being overcome, and many important and provocative experimental and theoretical results are now emerging, as reviewed recently by Sing and Perry [4]. Their review organizes the available theoretical approaches to the thermodynamics and structure of coacervates. These include the electrostatic “blob” theory in which the interacting units of the chains are multimonomer subcoils of the chain, as described in work by Rubinstein *et al.* [5]. This approach is likely only qualitative for dense coacervates. The case of

dense coacervates has been addressed using liquid state theory, which accounts for monomer-scale hard-core and electrostatic interactions, as exemplified in work by Perry and Sing [6] and by Wang and co-workers [7]. Both the blob theory and liquid state theory are “generic” in the sense that they use chemically nonspecific models in which polymer molecules are treated locally as either random-walk “blobs” or as spherical “monomers,” lacking chemical specificity other than size and effective van der Waals and Coulombic charge interactions. Chemical specificity can be provided in an *ad hoc* way through the assignment of chemically specific interaction free energies and Flory-Huggins Parameters between monomers and salt ions, which implicitly account for hydrogen bonding, hydrophobic effects, and other details through data fitting. Such an approach has been taken by Zhang and Shklovskii [8], de la Cruz *et al.* [9], Muthukumar and co-workers [10], and Salehi and Larson [11], the latter in collaboration with Friedowitz and Qin [12]. Rigorous, chemically realistic, analyses of the coacervate structure require atomistic simulations, as exemplified in work by Sammalkorpi, Lutkenhaus, and co-workers [13]. Such simulations are typically limited in the time and length scales they can access, and the detailed data they provide still need to be interpreted and generalized using more coarse-grained, or *ad hoc*, theories. Thus, all the above approaches will be valuable in filling out our understanding of the coacervate structure in the years ahead. For more details on these methods, the reader is referred to the review by Sing and Perry [4] and the papers referenced above.

This Review is directed specifically toward the *rheology* of coacervates and is intended to both summarize major findings and focus attention on where progress is most needed. We will focus on the linear rheology of coacervates made from two homopolyelectrolytes of the opposite charge, especially on data that satisfy “time-salt superposition,” which suggests some degree of “universality” in coacervate behavior. Readers are also directed to an overview by Liu *et al.* [1] of linear rheology, which also covers phase behavior briefly, as well as block polymer coacervates. There is also some recent work on *polyampholyte* coacervates, in which each polymer contains both a positively charged and a negatively charged block, with dynamics rather similar to that of mixtures of oppositely charged homopolyelectrolytes [14–16]. The review of Sing and Perry [4] mentioned above, not only focuses particularly on theories of equilibrium coacervation but also touches on rheology and other topics of current interest. Ultimately, theories should encompass both equilibrium phase behavior and rheology, since the same thermodynamic driving forces control them both. A validated theory of phase behavior would also allow the estimation of the compositional changes in the equilibrium coacervate phase when temperature, salt, or other variables are changed. This would help in interpreting the effect of these variables on the rheology of the equilibrium coacervate phase, including the “shift factors” discussed below.

Given the daunting complexities of coacervate rheology outlined above, a major boost was the discovery of the principle of the “time-salt superposition,” whereby the linear rheology curves (i.e., G' and G'' versus frequency) for coacervates with differing salt concentrations can be superposed onto a “master curve” by shifting along the frequency axis and to a

much lesser degree along the modulus axis. The time-salt superposition was first revealed clearly in the work by Cohen Stuart and co-workers [17,18] and has since been found in multiple coacervate chemistries, as we will see in this Review. However, a major caveat should be borne in mind. Frequently, coacervates are formulated by mixing the PEs with solvent and salt and allowing the coacervate to phase separate from a supernatant phase that contains not only water and salt but may also contain one or both PEs. As a result of the phase separation, the salt concentration in the coacervate can differ from that of the original mixture, and there can be differences in water and polymer concentrations as well, and possibly even a change in the ratio of monomer molarities of the two PEs as the overall salt concentration is changed. Consequently, the “time-salt superposition” involves the superposition of solutions differing at least somewhat in the PE concentration as well as in the salt concentration. These additional compositional variations introduce vertical shifting along the modulus axis, which is sensitive to the PE concentration and make the interpretation of the horizontal shift factors doubtful or complex since they are affected by PE concentration as well as salt concentration. There may also be doubt about the validity of the superposition itself, if it is carried out over a wide range of salt concentrations with only small overlaps of data. That is, large vertical and horizontal shifts may allow one to stitch together datasets for which the failure of the superposition would only have become evident if one had used wider frequency ranges. We will show an example of this later in the Review. The risk of a misleading “forced superposition” can be counteracted most effectively by using a wide frequency range at each salt concentration. A more efficient method is to use the time-temperature superposition to extend the frequency range. The latter method, while useful, carries its own risks, including the possibility of entering a two-phase region unwittingly, as might happen for the poly(diallyldimethylammonium)/poly(styrenesulfonate), PDADMA/PSS, which exhibits a surprising lower critical solution temperature [19].

In addition to these PE-specific issues, the quality of polymer synthesis and characterization is just as important in PE rheology as it is for the rheology of neutral polymers. In the literature to date, PE samples have usually been obtained from commercial vendors with higher polydispersities and less certainty regarding synthetic quality than is sometimes the case for more conventional polymers. We have assembled the information on polydispersity available from the publications or supplies, where available, in Table S2 in the supplementary material [69]. Generally, but not always, polydispersities range from $M_w/M_n = 1.1$ to 1.4. Even where synthesis and characterization of PEs are done in-house, with fractionation to reduce polydispersity, scrutiny, and replication of experimental results remain important tasks. While this Review does not address these experimental realities, readers should be aware that improved sample preparation and characterization will be a critical part of improving our understanding of coacervates and their rheology, and that conclusions drawn from data presented here may need revision as additional samples are studied.

To help the reader, we give in Table I abbreviations for the PEs (with polycations listed first) reviewed here, along with their pK_a values, monomer molecular weights M_0

(without including the molecular weight of any accompanying small salt ion), and literature-reported Kuhn lengths b_K .

The Review is outlined as follows: Sec. II discusses some suggested models of the coacervate structure. Section III describes the time-temperature superposition, and Sec. IV describes the time-salt superposition with multiple examples. Section V discusses the molecular weight dependence of zero-shear viscosity and terminal relaxation time, while Sec. VI describes the rheological consequences of large differences in the lengths of polycation (PC) versus polyanion (PA). Section VII discusses the time-salt-pH superposition, and Sec. VIII illustrates the time-hydration superposition. Section IX shows cases where a low-frequency plateau is present, and Sec. X covers available theories for coacervate rheology. Section XI summarizes the main conclusions.

II. STRUCTURE OF COACERVATES

It has long been recognized that a key driving force for PE complexation is the entropy gained by the release of small salt ions from a PE of given charge and replacement of these small ions by many fewer PE chains of opposite charge.

Recent theoretical and experimental works suggest that the complexation of a pair or a few long oppositely charged PEs occurs even in dilute solutions due to the small entropy loss caused by binding of a few chains together, relative to the huge entropy gain of the counterions thereby released [38,39]. Thus, the dense coacervate phase is likely in equilibrium with a supernatant phase containing dilute complexes each containing a few chains. Although coacervation produces close physical association of the PE molecules of opposing charge, the detailed organization of the PE chains within a coacervate has long been a matter of debate and speculation. Michaels [40] suggested both a “ladder model” in which two chains line up, pairing opposite charges like rungs of a ladder, as well as what to him seemed a more plausible “scrambled” model in which multiple polycations crisscross and associate with each polyanion and vice versa. It is well known that a single long PE in the solution takes on an expanded Gaussian conformation due to electrostatic repulsions at low salt; but with added salt, the screening of electrostatic interactions causes the coil to shrink down toward a size governed by its “bare” (or charge-free) Kuhn length, where the Kuhn length is the length of a random-walk step size of the chain. Indeed, neutron scattering

TABLE I. Relevant polycations/polyanions and their selected physical parameters.

Abbreviation	Polycation (or PC)	pKa	M_0 (Da)	b_K (nm)
PVP	Poly(4-vinylpyridine)	3–4.5 [20]	105	2.6 ^a [21]
PDMAEMA	Poly(<i>N,N</i> -dimethylamino ethyl methacrylate)	6.1–6.5 [17,18]	157	2.73, 3.66 ^b [22] 3.5, 16 [23]
PAH	Poly(allylamineH ⁺)	8.61–10.28 [24]	57	1.46–2.5 ^c [25]
PLK	Poly(L-lysine)	10.6 [26]	128	0.7 ^d [27]
PMAPTA	Poly[3-(methacryloylamino)-propyltrimethylammonium]	Strong	185	3.0 ^e [28]
PVBTMA	Poly[(vinylbenzyl) trimethylammonium]	Strong	176	—
PDADMA	Poly(diallyldimethylammonium)	Strong	126	5.0 ^f [29]
Abbreviation	Polyanion (or PA)	pKa	M_0 (Da)	b_K (nm)
PSS	Poly(styrenesulfonate)	1.22–1.50 [24]	183	3.0 ^g [30] 2.8–12 ^h [31]
PRE	Poly(D, L-glutamic acid)	5 ⁱ [32]	129	0.7 ^d [27]
PAA	Poly(acrylic acid)	5–5.5 [18] 4.79–5.78 [24]	72	0.64 ^j [33] 0.86–2.52 ^k [25] 6.3 [23] 11.7 ^l [34]
IBMA	Poly(isobutylene-alt-maleate)	6.4 [35]	170	0.68–0.79 ^m [36]
PMA	Poly(methacrylic acid)	7.03 [24] 6.4 [35]	86	0.6 ⁿ [37]

^aEvaluated in the HCl solution by light scattering using the wormlike chain (WLC) theory.

^b2.73 nm is for unionized PDMAEMA in methanol, 3.66 nm is for ionized PDMAEMA•HCl.

^cUsing the WLC relationship and atomistic molecular dynamics, the persistence length varied from 0.73 nm (at 0% ionization) to 1.25 nm (at 100% ionization).

^dMeasured at 5 wt. % polymer concentration without salt by small-angle x-ray scattering.

^eAssumed by Yang *et al.* [28] because the Kuhn length of a PC similar to PMAPTA in a PEC in 1M NaCl was reported to be 3 nm.

^fMeasured in 0.5M NaCl solution by light scattering.

^gEstimated in 0.5M NaCl solution by light scattering.

^hThe persistence length measured by small angle neutron scattering was from 1.4 (in 3M NaBr solution) to 6 nm (without salt).

ⁱEstimated from Fig. 3 in Appel and Yang [32].

^jCalculated using the freely joint-chain (FJC) model together with the force-extension curve measured by atomic force microscopy.

^kThe electrostatic persistence length, calculated according to the WLC relation and full atomistic molecular dynamics simulations, was from 0.43 nm (at 0% ionization) to 1.26 nm (at 100% ionization).

^lMeasured by small-angle x-ray scattering for un-neutralized PAA in water at 25 °C.

^mThe Debye length of IBMA is estimated as 0.68–0.79 nm, which is claimed to be consistent with the Kuhn length of IBMA.

ⁿEstimated in the mercapto and dodecanol solution without salt from the fits of WLC and FJC models using atomic force microscopy.

studies by Schlenoff and co-workers [41] on solutions of PSS show, as expected, that the coil size is expanded at low ionic strength but shrinks toward the bare (charge-free) size with increasing added salt, where the bare PSS Kuhn length is around 1.4 nm. In coacervates of PSS with PDADMA, the ionic strength due to the PE alone is high, and the same group [42] finds that the coil size is small and insensitive to the added salt concentration, as one might expect. More recent neutron scattering results by Schlenoff and co-workers [43] show that in coacervates of poly[3-(methacryloylamino)-propyltrimethylammonium]/poly(methacrylic acid) (i.e., PMAPTA/PMA), the deuterated PMA chains have Gaussian configurations with Kuhn lengths of 1.5 nm similar to that of the bare PSS Kuhn length. This evidence supports the “scrambled” model of the coacervate with chains of both PEs taking on Gaussian configurations with Kuhn lengths similar to those of the corresponding uncharged polymers. However, Spruijt *et al.* [23] found that in coacervates of poly(*N,N*-dimethylamino ethyl methacrylate)/poly(acrylic acid), or PDMAEMA/PAA, Kuhn lengths obtained from radii of gyration measured by neutron scattering were 3.5 and 16 nm for the two different chain lengths of PDMAEMA, and 6.3 nm for PAA. These values are larger than one would expect for the bare Kuhn length, but Spruijt *et al.* commented that these values are “upper bounds” due to possible bias from the radii of gyration of long chains selectively segregating to the coacervate. Estimated Kuhn lengths for various PEs under different conditions of salinity, *pH*, and solvent conditions are given in Table I. Even if the configurations of chains in the coacervate are random walks with small Kuhn lengths, the nature of the interactions of the charges on the chains remains in doubt. One limiting possibility is that the arrangement of the charges on the chains is similar to that of simple salt charges, with opposite charges correlated to reduce spatial variations in net charge and electrostatic energy, while allowing the considerable positional disorder to maintain high entropy. This picture is the basis of the Voorn–Overbeek theory of coacervation [44], which ignores the connectedness of polymeric charges, treating them as simple salt ions when calculating their electrostatic interactions.

While this simplistic picture is now largely superseded by theories that more realistically account for chain connectivity, the possibility remains that each polymeric ion sees a “cloud”

of neighboring oppositely charged monomers or salt ions, as opposed to being neutralized by one and only one charge on a neighboring oppositely charged monomer or salt ion, forming a so-called “ion pair” or condensed salt ion. In the latter case, the breakage time of the ion pair is the fundamental event governing the relaxation dynamics of the coacervate. An intermediate possibility, suggested by Colby and co-workers [36], is that oppositely charged chains are paired up for long periods of time as depicted in Fig. 1 and that the time constant for the reorganization of the coacervate is determined by the rates of formation and breakage of “quadrupolar” local groupings of chains, as depicted in Fig. 1. This depiction has the advantage that it accommodates significant differences in spacing of charges on the two chains, with the “wavy” red chain having a wider spacing of charges than the black chain. However, the depiction suggests an extended or expanded conformation of the chains, which seems at odds with at least some neutron scattering data [43]. Lytle and Sing [45] have developed a modification of the ion-pairing picture wherein the binding of one monomer of a PE chain to an oppositely charged chain biases the next monomers on these two chains to bind also. The enhanced probability of binding of the second monomer was expressed in terms of a “transfer matrix” whose probabilities could be deduced from coarse-grained molecular simulations. It is also possible that a more helpful picture might be that of the association of multiple monomers, salt ions, and waters of hydration, whose cooperative motions are necessary for motion of a single monomer, similar to the situation for many glasses, as suggested by some experiments and simulations [13,43].

For better or worse, the detailed structure of the coacervate does not seem to have been of great concern in the development of models for the rheological properties, which are generally of the “sticky diffusion” type, whose rheological predictions are governed by rates of local diffusion. While dependences of these rates on temperature, salt concentration, and other variables can be extracted from fitting the models to experimental data, these dependencies do not define the mechanisms of local relaxation, nor do they even require that diffusion be of the “sticky” type, since any other local mechanism of relaxation, including highly cooperative ones, would give the same rheological phenomena at longer time scales. It can be questioned how well “sticky diffusion” concepts really apply to coacervates composed of two types

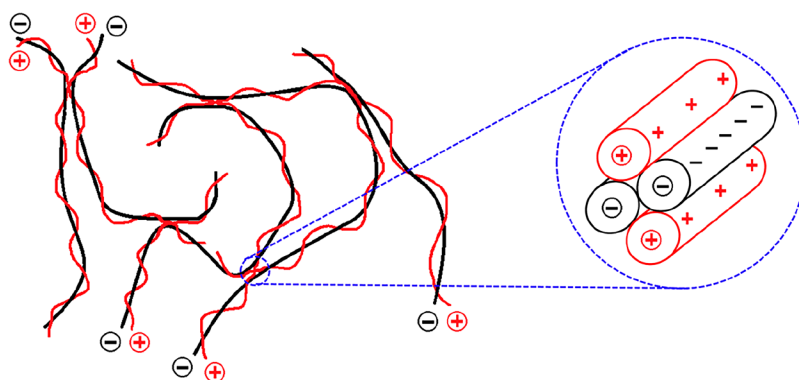


FIG. 1. Schematic of possible polycation (red, wavy line, positively charged) and polyanion (black) conformations in coacervates [36]. Used with permission from Hamad *et al.*, *Macromolecules* **51**, 5547–5555 (2018). Copyright 2018, American Chemical Society.

of polymers. The flexibility of the models to fit rheological data means we can interpret these data without too much regard for either the detailed microstructure or the local dynamics, but, of course, this also limits our ability to use rheology to deduce the structure or local interactions. This is a familiar conundrum, in which rheology has exquisite quantitative, but limited qualitative, value. Combined with structural information, for example, from scattering measurements or simulations, however, rheology can in principle generate substantial insight into both the structure and rates of structural change. In the future, the combination of macroscopic rheology and incisive structural probes will hopefully provide a rich picture of the coacervate structure and dynamics from small scales to large. Of primary concern here, however, is the rheological data and their interpretation in terms of rheological models. We, therefore, proceed directly to the description of the available rheological data and then to its modeling. We will return to the local structure and dynamics in Sec. X.

III. TIME-TEMPERATURE SUPERPOSITION

The well-known principle of time-temperature (t-T) superposition is illustrated in Fig. 2 for a coacervate of PMAPTA and PMA for various degrees of polymerization n_{av} , chosen

to be roughly equal for PC and PA. Figure 2 includes results for three different concentrations of NaCl, the lowest being near zero. The different colors (or shades in black and white) index the temperatures used, and for each temperature, “horizontal” and “vertical” shift factors, a_T and b_T , respectively, are employed to bring the curves into superposition on a log-log scale to form a pair of “master curves” for G' and G'' for each coacervate. The vertical shift factor reflects a change in modulus with temperature and only slightly deviates from unity over the temperature range from -5 to 65 °C. The horizontal shift factor a_T , on the other hand, varies with temperature by over four orders of magnitude for low salt and 1.5 orders of magnitude for 0.3M NaCl, following an Arrhenius dependence as shown in Fig. 3 for one of the five pairs of molecular weights.

The superposition of results at different temperatures indicates that the relaxation processes in the coacervate are the same at each temperature, apart from a rate factor that acts as a “metronome” that uniformly speeds up (or slows down) all processes by the same relative amount as temperature increases (or decreases). The success of the superposition indicates that temperature controls primarily the local friction but otherwise changes little or nothing about the solution structure or the processes by which relaxation

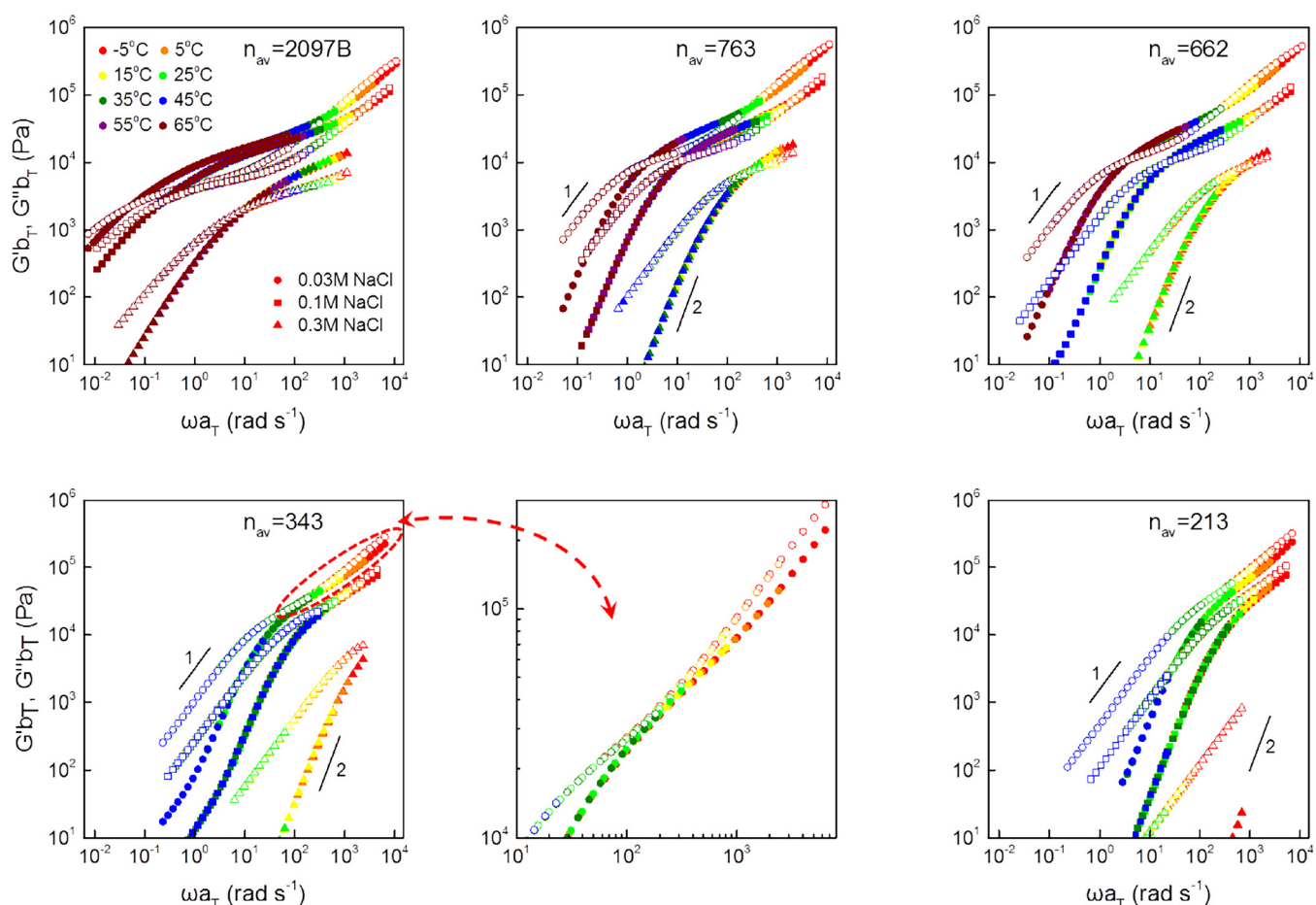


FIG. 2. Time-temperature superposed storage (G' , solid symbols) and loss (G'' , open symbols) moduli for coacervates of in-house synthesized PMAPTA and PMA with average degrees of polymerization n_{av} at three NaCl concentrations 0.03M (\bullet , \circ), 0.1M (\blacksquare , \square), and 0.3M (\blacktriangle , \triangle). The horizontal shift factor a_T is given in Fig. 3 below, with reference temperature = 25 °C. The vertical shift factor b_T varies only about 10% from unity and decreases with increasing temperature as expected. The center lower panel magnifies the high-frequency portion of the data for $n_{av}=343$ [28]. Used with permission from Yang *et al.*, *Macromolecules* **52**, 1930–1941 (2019). Copyright 2019, American Chemical Society.

occurs. Similar t-T superposition is commonly observed in the relaxation of neutral homopolymers, such as polybutadiene, polystyrene, polyethylene, etc. [46], although deviations from superposition can often be observed at high frequencies and high values of G' and G'' (typically above 10^7 Pa in melts). At these high frequencies, local spatial heterogeneities in modes of relaxation having different temperature dependencies are not sufficiently averaged together to produce a single “mean field” friction [47]. Similar failures of the t-T superposition may occur in coacervates if very high frequencies, beyond those reached in Fig. 2, are accessed. Interestingly, in heterogeneous polymers such as mixtures of different homopolymers, the t-T superposition typically fails, over all frequencies [46,48] presumably because the two polymeric components, even if miscible, are locally segregated enough for the differing temperature dependencies of the frictional contributions of each to express even at modest or low frequency. Given the failure of the t-T superposition typical in even miscible blends of uncharged homopolymers [49], it may seem surprising that the t-T superposition would hold in a coacervate containing two chemically very different PEs. One may interpret this as evidence that the two PEs are intimately mixed due to their attractive charge interactions, with both chains “pooling” their frictional response to produce an effective single friction coefficient that reflects the contributions of both chains, at least over the range of frequency for which the t-T superposition holds.

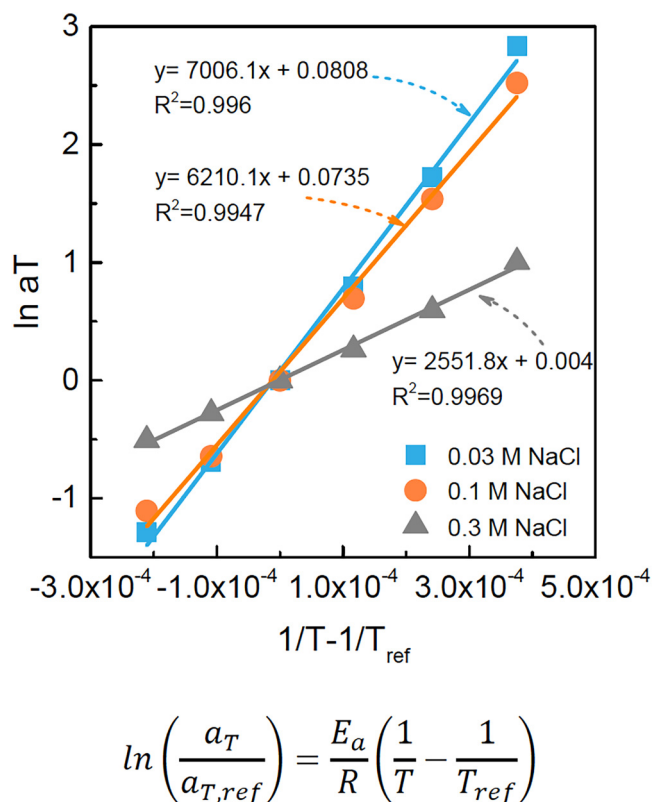


FIG. 3. Arrhenius plot of temperature dependence of shift factor a_T for the $n_{av} = 2097B$ sample from Fig. 2 at the three salt concentrations, with reference temperature = 25 °C [28]. Used with permission from Yang *et al.*, *Macromolecules* **52**, 1930–1941 (2019). Copyright 2019, American Chemical Society.

Note in Fig. 3 that the dependence of the shift factor a_T on temperature follows an Arrhenius form, which is exponential in the inverse of temperature. This, very common, temperature dependence normally reflects relaxation that is controlled by a single activated process, characterized by an “activation energy” E_a that needs to be overcome to allow a single “elementary” step in the relaxation to occur. The value of E_a in an Arrhenius fit is, therefore, a clue to the key processes that allow relaxation to occur. The Arrhenius form is typical for polymeric melts at temperatures much higher (≈ 100 °C higher) than their glass transition temperature; at lower temperatures within 50–100 °C of their glass transition, the so-called “WLF” form is observed for most polymeric melts [46]. (The WLF form is thought to arise from increasingly cooperative relaxation upon cooling and densification so that there is no single activation energy governing relaxation.) It is instructive that the activation energy for the coacervate of Figs. 2 and 3 decreases dramatically from around $23 k_B T$ to $21 k_B T$ to $9 k_B T$ (corresponding to 58, to 51 to 21 kJ/mol), as the salt concentration increases from 0.03 to 0.10, to 0.30M. Yang *et al.* [28] have suggested that the “elementary” step governing coacervate relaxation, in the absence of salt, involves four monomers, as depicted in Fig. 4(A). In this picture, local movements of a charged monomer require breaking of its physical “bond” with an oppositely charged monomer on another chain. In the absence of salt ions, or of unbound charged monomers, two such bonds must exchange partners in a coordinated fashion [36] to enable the “hopping” of a monomer from one chain to another as illustrated in Fig. 4(A), with consequent large activation energy. The addition of salt enables the hopping of one monomer to occur independently of its former partner

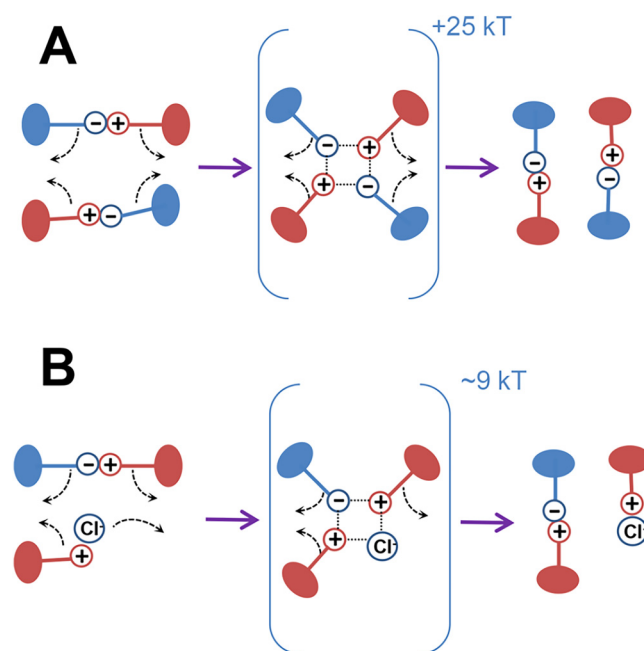


FIG. 4. Proposed elementary mechanism of viscoelastic relaxation involving polyanion monomers (blue dots denoted with “-”) and polycation monomers (red dots denoted with “+”), without (A) and with (B) enablement by salt ion binding [28]. Used with permission from Yang *et al.*, *Macromolecules* **52**, 1930–1941 (2019). Copyright 2019, American Chemical Society.

monomer, as illustrated in Fig. 4(B), with much lower activation energy. This speculative picture assumes that unbound monomer charges are rare and that coordinated motions of monomers and salt ions more complex than those of Fig. 4 are unimportant. However, more complex exchange processes would give a similar t-T shifting, as long as the mix of underlying basic processes stays the same at other temperatures. Hence, until the activation energy and its dependence on the salt concentration are explained quantitatively, considerable uncertainty must be ascribed to any putative mechanism of relaxation.

IV. TIME-SALT SUPERPOSITION

The first clear demonstration of the time-salt (t-s) superposition, shown in Fig. 5, was the work of Cohen Stuart and co-workers [18] for poly(*N,N*-dimethylamino ethyl methacrylate) (PDMAEMA) and PAA at near-neutral pH where both PEs are almost completely charged. This work of Spruijt *et al.* covered a range of degrees of polymerization, $N = 20, 50, 100, 150,$ and $510,$ and salt concentrations, $0.5, 0.75, 1.05, 1.2\text{M}$ KCl. They plotted curves of $G'_{\text{scaled}} = G' / G_c$ and $G''_{\text{scaled}} = G'' / G_c$ against $\omega_{\text{scaled}} = \omega \tau_c$ with salt-dependent horizontal shift factor τ_c and vertical shift factor G_c . (In Fig. 5, the low-frequency limiting power law slopes of 1 and 2 for G'' and G' are used to extrapolate these G'' and G' curves until they cross, and G_c and τ_c are the modulus and inverse frequency at this crossing point.) Others have shown the t-s superposition for other coacervates including the PMAPTA/PMA coacervates of Schlenoff and co-workers [28] presented in Fig. 2, whose t-s superposition is shown in Fig. 6. The time-salt superposition typically requires larger vertical shift factors than are used in the t-T superposition, in part, because the polymer concentration is usually not held constant as salt concentration is changed. For example, in Fig. 6, the polymer volume fraction varies from $\phi = 0.298$ to 0.203 to 0.154 with salt concentration increasing from $[\text{NaCl}] = 0.03$ to 0.10 to 0.30M . Counteracting this decrease in polymer concentration requires shifting the G' and G'' curves vertically upward by almost a factor of two in some cases [28]. Still, the horizontal shift factors are much more significant than the vertical ones, ranging over two decades as shown in the last panel of Fig. 6.

While the apparent success of the time-salt superposition greatly simplifies our physical interpretation of salt effects on rheology, one should be cautious in assuming that the superpositions are really as good as they seem. Often master curves spanning six to eight decades of frequency are constructed from measurements that span only two to three decades each, as is evident in the ranges of each colored symbol in Fig. 5. Extensive studies of the time-temperature superposition in conventional polymer melts have revealed significant deviations from the t-T superposition that only become evident when very wide ranges of frequency or time are scanned at each temperature. It is likely that similar deviations from the time-salt superposition will also be revealed once wide frequency or time ranges are scanned for coacervates, for example, using creep tests. Even existing datasets, for example, in Fig. 6 at low frequency, show failures in the overlap of data points, which are telltale signs of the imperfect superposition. While the

usefulness of superposition for semiquantitative or qualitative analysis makes it worth exploiting whenever possible, the limitations of the method should be kept in mind and efforts should be made to quantify deviations and failures. An example of a likely severe failure that is uncovered by the use of wider frequency ranges at each salt concentration will be discussed below in connection with Figs. 18–20. Similar caution should be used in the other superpositions discussed below.

In the time-salt master curves of both Spruijt *et al.* [18] in Fig. 5 and of Yang *et al.* [28] in Fig. 6, the degrees of polymerization (defined as “ N ” in Fig. 5 or “ n_{av} ” in Fig. 6), were chosen to be nearly the same for the two polyions in the coacervate. An exception is in Fig. 5(e), where the two polyions differed in N by a factor of three. Notice that at the lowest degrees of polymerization, below around 150 in Figs. 5(a)–5(c), the storage modulus for PDMAEMA/PAA remains below the loss modulus for dimensionless frequencies $\omega \tau_c$ extending at least up to 10^2 , while for N around 500, there is a crossover in which G' exceeds G'' and flattens its slope shortly beyond the crossover frequency. Somewhat similar behavior is observed for PMAPTA/PMA at the highest average degree of polymerization n_{av} in Fig. 6, although the flattening is less distinct and requires a higher n_{av} to be observed. This behavior is highly reminiscent of the transition in neutral polymer solutions from unentangled to entangled polymer rheology, with the flattening of the G' curve suggesting a transition to an entanglement network at high molecular weight [46]. For neutral polymers, the transition molecular weight at which entanglements appear is related to the modulus along the plateau. For the data of Spruijt *et al.*, the characteristic modulus G_c is reported to decrease from around 10^4 to 10^3 Pa, as N increases to 500 so that from Fig. 5(d), one infers a “plateau” modulus of around 10^5 Pa. For the data of Yang *et al.* [28], the “plateau” is at around 2×10^4 Pa.

If the plateau discussed above is produced by entanglements, its modulus G_0 should be related to the entanglement molecular weight M_e roughly by

$$G_0 = \phi \rho RT / M_e, \quad (1)$$

where ρ is the polymer bulk density (i.e., without the solvent) and ϕ is the polymer volume fraction so that $\phi \rho$ is the solution polymer density; M_e is the entanglement molecular weight in the solution, R is the gas constant, and T is the absolute temperature. (The entanglement molecular weight in the solvent-free bulk polymer is designated “ $M_{e,0}$.”) A brief discussion of the entanglement molecular weights inferred from the rheology can be found in the SI [69].

Results in Fig. 7 for even higher molecular weights of PMAPTA/PMA with n_{avg} up to nearly 5000, at nearly zero salt concentration, show the further development and lengthening of the plateau region, with nearly constant plateau modulus, G_0 . The polymers used to acquire these data were also more nearly monodisperse than for those in Fig. 6, with $M_w/M_n \leq 1.06$ for PMAPTA and ≤ 1.15 for PMA in Fig. 7. (The corresponding values of M_w/M_n in Fig. 6 are 1.27 and 1.06 but with 1.75 and 1.41 for the longest chains.) Notice that the high-frequency behavior in both plots, above a

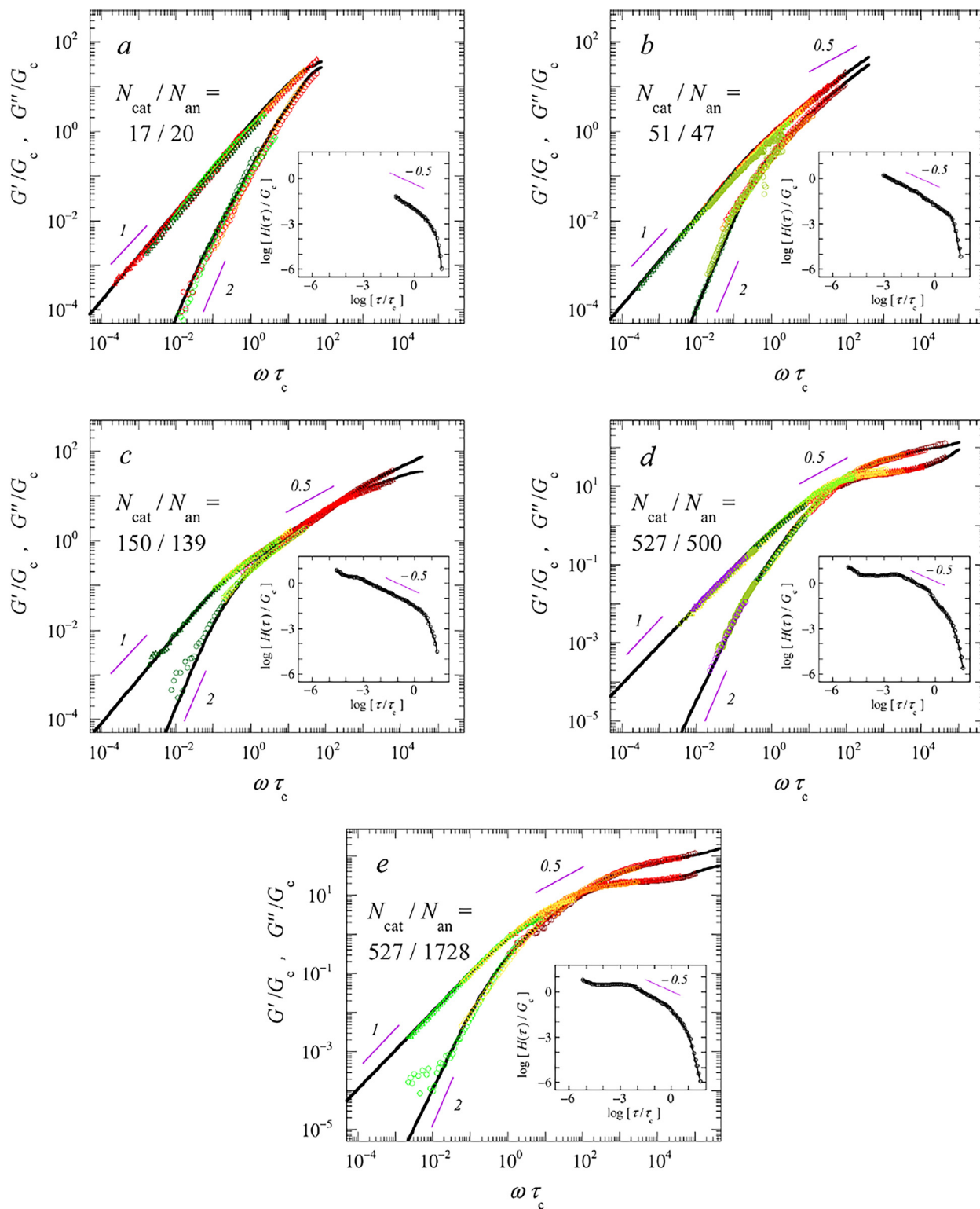


FIG. 5. Time-salt frequency-shifted linear viscoelastic curves for PDMAEMA/PAA/KCl coacervates for different PC/PA degrees of polymerization, $N_{\text{cat}}/N_{\text{an}}$, given in the legends. The shift factors τ_c and G_c are taken from the inverse frequency and modulus at which G' s and G'' cross each other, when extrapolated from the low-frequency viscous limit. Thus, by definition, at $\omega\tau_c=1$ and $G'/G_c=1$, with G_c decreasing from 10^4 to 10^3 Pa as molecular weight increases. The insets give logarithmic relaxation time spectra. Colors (or shades in black and white) mark data at different salt concentration [18]. Used with permission from Spruijt *et al.*, *Macromolecules* **46**, 1633–1641 (2013). Copyright 2013, American Chemical Society.

shifted frequency of around 100 rad/s, is almost independent of molecular weight. This shows that the fast “elementary” relaxation processes are independent of the chain length. The success of time-temperature shifting implies that all slower processes are the result of combinations of these elementary

processes throughout the coacervate. Not only is the mechanism of local relaxation of interest, but it is also important to determine how the accumulation of these fast local processes leads to slower relaxations and ultimately to complete relaxation of the coacervate at long times.

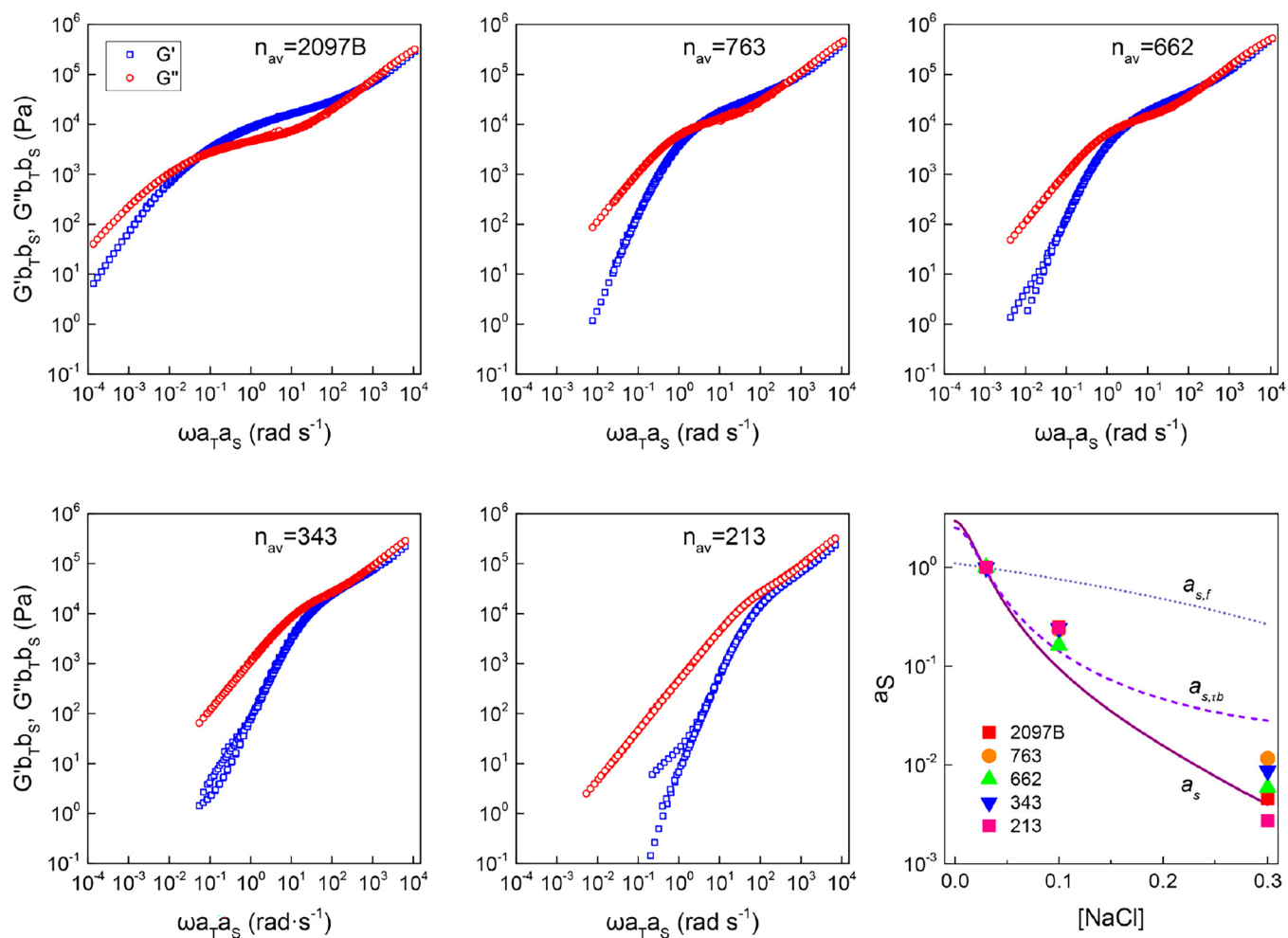


FIG. 6. Time-temperature-salt superposition obtained for coacervates of in-house synthesized PMAPTA /PMA by further shifting data of Fig. 2 by a factor a_s along the frequency axis and b_s along the modulus axis, with G' (\square); G'' (\circ). The lower right figure gives a_s as a function of NaCl concentration for the different average molecular weights. The shift factor a_s is taken to be the product of $a_{s,tb}$, due to the sticker lifetime, a_f , due to the fraction of stickers, and a_ϕ , due to changes in polymer concentration. The third of these is estimated as $a_\phi = \phi/\phi_{ref}$ while estimates for the other two are given by Yang *et al.* [28]. The “B” in “2097B” indicates that this sample is composed of PEs with “broad” molecular weight distributions of 1.75 for PMAPTA and 1.41 for PMA. The other samples have “narrow” molecular weight distributions of less than or equal to 1.27 for PMAPTA and less than 1.06 for PMA [28]. Used with permission from Yang *et al.*, *Macromolecules* **52**, 1930–1941 (2019). Copyright 2019, American Chemical Society.

Very recently, Syed and Srivastava [50] have shown that the relevant “salt concentration” governing the shifting of linear rheology is the total ionic strength of the small ions, including the counterions to the polymer itself. They showed this in a coacervate of poly(allylamine hydrochloride) (PAH) and PAA, each of molecular weight around 15 kDa by changing both the *overall* added salt concentration at fixed PE concentrations and by changing the *overall* PE concentration at fixed added salt concentration. The “*overall* concentrations” are those of the prepared solution, which then phase separates into a coacervate and a supernatant solution. Changing either the overall salt or overall PE concentration shifts both the composition of the coacervate and the phase volume of the coacervate, where the latter is essentially the position along a tie line of the two-phase envelope. For the compositions studied by Syed and Srivastava [50], the PE concentration changed little with changing overall polymer or salt concentration, and the major difference in all coacervates was simply the concentration of small salt ions. The total ionic strength of both the coacervate and supernatant could thus be varied either through changing the added overall

salt concentration or the overall PE concentration. Both methods produced the same master curve when the shift factor was made to depend on the overall ionic strength of the small ions, both those of the added salt and the counterions of the PE solution. The shift factor due to both changes in overall added salt concentration, a_s and due to changes in overall polymer concentration, a_p , resulted in a master curve with the shift factor that depended on overall small-ion ionic strength, I , as $a_s a_p \sim \exp(-4.47 I^{1/2})$. As alluded to in the introduction, however, it should not be assumed that, in general, the effect of salt on PE concentration can be ignored. In some cases, there may be changes large enough to affect the rheology.

V. MOLECULAR WEIGHT DEPENDENCES OF ZERO-SHEAR VISCOSITY AND TERMINAL RELAXATION TIME

A major clue to understand the long-time dynamics is in the scaling of the longest relaxation time and zero-shear viscosity with chain length. In the PDMAEMA/PAA coacervates

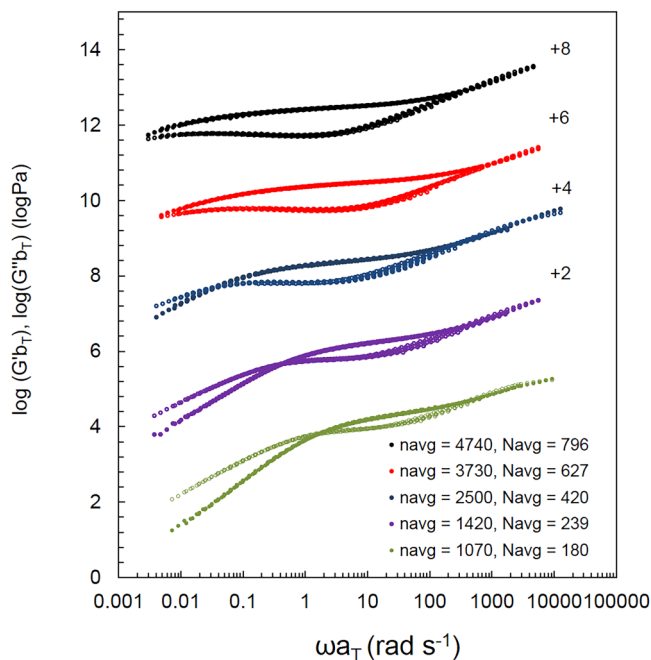


FIG. 7. Time-temperature superposed G' and G'' for coacervates of in-house synthesized PMAPTA/PMA with 0.01M NaCl having average degrees of polymerization n_{avg} and numbers of Kuhn steps $N_{avg} = n_{avg}/5.9$ at reference temperature °C. Each curve except the one for $n_{avg} = 1070$ has been shifted upward by the indicated number of log frequency units (2, 4, 6, or 8) [43]. Used with permission from Akkaoui *et al.*, *Macromolecules* **53**, 4234–4246 (2020). Copyright 2020, American Chemical Society.

of Spruijt *et al.*[18], the longest relaxation time τ was found to scale with the square of average molecular weight at salt (KCl) concentration 0.6M, from the lowest average chain length of 40 up to the highest of $n_{av} = 10^3$ monomers. A similar quadratic scaling of zero-shear viscosity η_0 was found for salt concentrations in the range 0.5–0.7M KCl, while a roughly linear scaling of η_0 with chain length was found at 1.0M KCl. The quadratic scaling of τ with chain length agrees with the Rouse theory for unentangled polymers, but the quadratic scaling for η_0 for 0.5–0.7M KCl disagrees with the linear scaling of η_0 expected for unentangled polymers at constant polymer volume fraction. However, Spruijt *et al.* [18] noted that the polymer volume fraction increased “moderately” with increasing chain length (a range of ϕ in their samples from 0.05 to 0.30 was noted but its molecular weight dependence was not clearly delineated), and perhaps this could explain the shift from linear to quadratic scaling of η_0 with n_{av} . However, the transition to what appears to be an entangled polymer regime is evident in the shape of the G' curve at the longest chain lengths [see Figs. 5(d)–5(e)], and this does not seem evident in the scaling of zero-shear viscosity. Perhaps, this is because the entangled regime has not been entered into very deeply and because changes in the scaling laws of η_0 and τ with chain length are obscured by simultaneous changes in polymer concentration.

For PMAPTA/PMA coacervates, Figs. 8 and 9 show the dependences of the zero-shear viscosity on average chain length from two studies of Schlenoff and co-workers [28,43], the first covering a range of n_{avg} up to 2097, and the second reaching a higher value of 4740. (Note that the conversion of

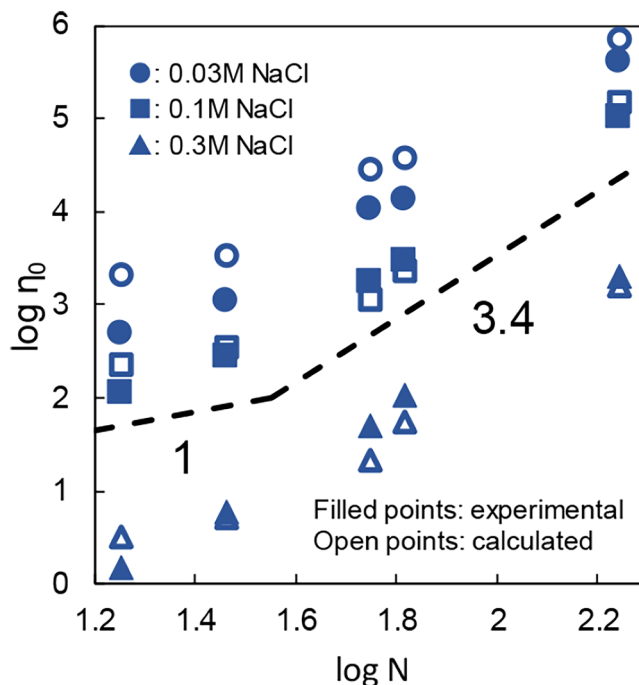


FIG. 8. Zero shear viscosity η_0 at 25 °C of PMAPTA/PMA PECs as a function of number of Kuhn steps at salt concentrations given in the legend at 25 °C. Here, the number of Kuhn steps N is related to the degree of polymerization by $N = n_{av}/11.9$, where n_{av} is the number of monomers. Filled symbols are experimental, and open symbols are calculated from the product of Rouse relaxation time τ_R and Rouse modulus G_R for $N \leq N_c$ and of plateau modulus G_0 and reptation time τ_d for $N > N_c$, where N_c is estimated as 29 [28]. Used with permission from Yang *et al.*, *Macromolecules* **52**, 1930–1941 (2019). Copyright 2019, American Chemical Society.

the values of n_{avg} to numbers of Kuhn lengths N is different in Figs. 8 and 9, with $N = n_{avg}/11.9$ in Fig. 8 but $N = n_{avg}/5.9$ in Fig. 9. Note also that Schlenoff and co-workers use “ N ” to denote the number of Kuhn steps in the chain, while Cohen Stuart *et al.*[18] use “ N ” for the number of monomers, which is “ n_{avg} ” or “ n_{av} ” in the work of Schlenoff *et al.* [28,43]. This difference between the two publications by the Schlenoff group resulted from the authors’ reassessment of the value of the Kuhn length, estimated to be 2 nm in Yang *et al.* [28] but reassessed to be 1.5 nm in Akkaoui *et al.* [43].) Figure 8 shows a transition from a power-law exponent of around unity to 3.4 in the dependence of zero-shear viscosity on N ; the transition occurs at a value $N \approx 30$, which is $n_{avg} \approx 360$ when we convert from N to n_{avg} using the ratio 11.9 mentioned above. In Fig. 9, an even steeper power-law of 5.4 is observed for N above 180, which corresponds to $n_{avg} \approx 1000$. The transition from unity to 3.4 is expected based on the transition to the entangled state, which we noted above should occur at $n_{avg} \approx 300$ –450, for the data in Figs. 8 and 9. The onset of the entangled state thus seems to correspond to a transition to the region of 5.4 power law in Fig. 10, and the half-decade wide region with “3.4 power law” marked in Fig. 8 then likely just reflects a broad transition from a region with power law near unity to a region with a power law of 5.4. The power law exponent of 5.4, however, is anomalous, since rheology dominated by entanglements should lead instead to a power law of around 3.4 at high molecular weights. Electrostatic interactions, manifested

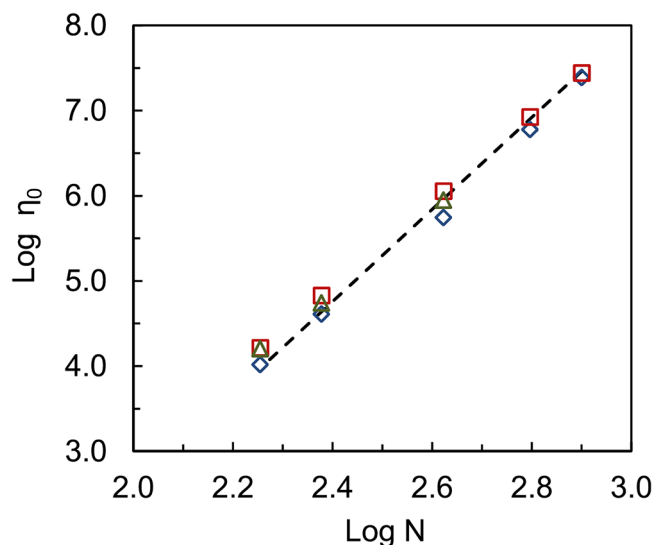
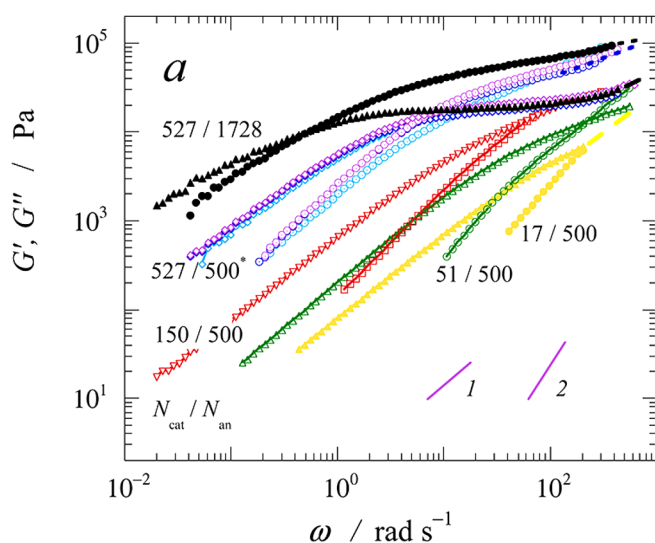


FIG. 9. Zero-shear viscosity η_0 at 25 °C of PMAPTA/PMA coacervates versus number of Kuhn steps, $N = n_{\text{avg}}/5.9$, between 180 and 796, from direct measurements (Δ), from the product $G_0\tau_{\text{rep}}$ of the measured plateau modulus G_0 and measured longest relaxation time τ_{rep} (\diamond), and calculated from the product of theoretical expressions for these (\square). The dotted line gives the scaling law $\eta_0 \sim N^{5.4}$ [43]. Used with permission from Akkaoui *et al.*, *Macromolecules* **53**, 4234–4246 (2020). Copyright 2020, American Chemical Society.

as ion pairs, or other restrictions on polymer local mobility, can certainly slow chain dynamics, but no matter how strong these effects, they should not change the power-law scaling of viscosity with molecular weight, as long as they *act locally* so that the dynamics of the whole chain are slowed to the same degree regardless of chain length. A change in power law exponent at high molecular weight from 3.4 to 5.4 seems therefore to imply that the electrostatic interactions lead to a chain-length-dependent slowdown in local dynamics. A mechanism for this suggested by Akkaoui *et al.* [43]



involves a kinetic coupling of ion-pairing and entanglement dynamics, but this suggestion at present remains untested. We also note the seeming discrepancy between the molecular-weight-scaling behavior of PDMAEMA/PAA of Spruijt *et al.* [18], and that of PMAPTA/PMA of Schlenoff and co-workers. Since the PEs studied by Spruijt *et al.* neither reached degrees of polymerization as high as those studied by Akkaoui *et al.*, nor were they as monodisperse, further experimental work will be needed to resolve whether these two systems actually behave differently.

VI. EFFECT OF UNEQUAL DEGREES OF POLYMERIZATION

The above results focused on coacervates in which both PEs had similar chain lengths. Results from Spruijt *et al.* [18] in Fig. 10 show the relaxation behavior of PDMAEMA/PAA coacervates for which the two lengths are significantly different. Figure 10(a) shows that increasing the polycation, PDMAEMA, length at a fixed length of the polyanion, PAA, greatly slows the relaxation, while the reverse case in Fig. 10(b) shows much less effect of the length of PAA with fixed PDMAEMA length, at least until the PAA becomes very long. This seems to show that the terminal relaxation is dominated by the motion of the PDMAEMA, with the PAA serving primarily to impede this relaxation, while not itself significantly contributing to the terminal relaxation until the PAA is very long. This behavior seems hard to explain in terms of a simple ion-pairing model, where the release of an ion pair should have an equal effect on the local relaxation of each chain, and therefore lead to equivalent behavior, whenever either chain is made longer than the other. On the other hand, for coacervates of PDADMA and poly(isobutylene-alt-maleate sodium) (IBMA-Na) studied by Hamad *et al.* [36], Fig. 11 shows that the polyanion, IBMA ($pK_a = 3.2\text{--}3.3$) [35], strongly influences the terminal relaxation behavior, differing from the

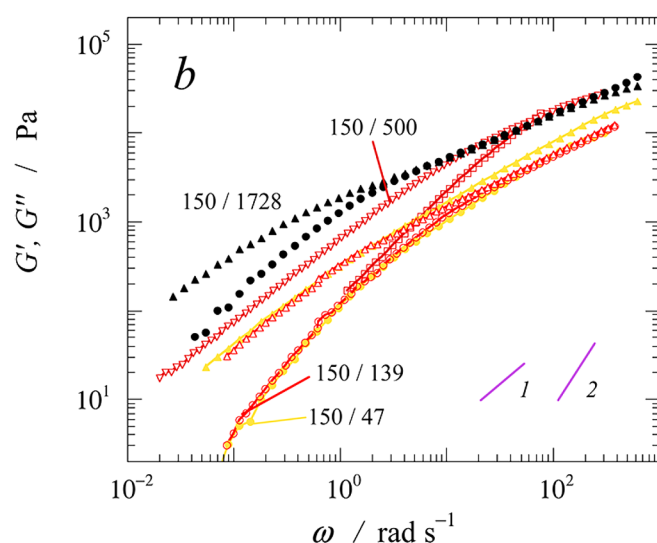


FIG. 10. Linear rheology of PDMAEMA/PAA coacervates in which degrees of polymerization (N) of each PE varies as shown. In (a), $N = 500$ for PAA, and PDMAEMA has varying $N = 17, 51, 150, 527$, except for the black (farthest left) symbols, which have the N values 527/1728. The curves with the label “527/500*” denote the cases 527/500, 527/139, 527/47, and 527/20, which overlap [18]. In (b), $N = 150$ for PDMAEMA, while N for PAA varies as shown. All results are at 0.70 M KCl at roughly 1:1 monomer mole ratio of the two polymers. Used with permission from Spruijt *et al.*, *Macromolecules* **46**, 1633–1641 (2013). Copyright 2013, American Chemical Society.

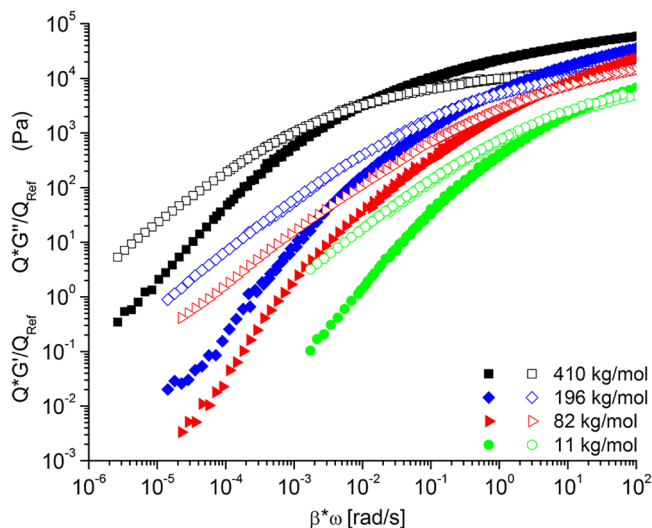


FIG. 11. Master time-salt superposition curves of G' (filled symbols) and G'' (open symbols) of coacervates of PDADMA and IBMA with the salt-free coacervate as the reference state at 23 °C molecular weight of PDADMAC = 300 kDa, and the molecular weights of IBMA-Na shown [36]. Used with permission from Hamad *et al.*, *Macromolecules* **51**, 5547–5555 (2018). Copyright 2018, American Chemical Society.

PDMAEMA/PAA system studied by Spruijt *et al.* In very recent work, Liu *et al.* [51] studied coacervates of cationic poly([2-(methacryloyloxy)ethyl]trimethylammonium) (PTMAEMA) with anionic poly(3-sulfopropyl methacryloyl) (PSPMA) of mismatched lengths, and, as in the study of Spruijt *et al.*, found a somewhat greater influence of the length of the cation on the rheology than of the anion, although not to the degree seen by Spruijt *et al.* for PDMAEMA/PAA. The

reason for these differing behaviors needs resolution, and a possible reason for this asymmetry in some systems may lie in asymmetry in the Kuhn lengths of PC versus PA, as suggested below in the theory section.

From both Figs. 10 and 11, we can estimate $G_0 \approx 5 \times 10^4$ Pa, suggesting from Eq. (1) that $M_e \approx 10$ kDa for both. In Fig. 10(a) the cross over frequency shifts roughly fourfold for a threefold increase in degree of PDMAEMA polymerization from $N = 51$ to 150 and roughly a decade additional increase for a further threefold increase to 527, suggesting a quadratic dependence on N for PDMAEMA at long chain lengths, which suggests that the chains are unentangled. Consistent with this, for PDMAEMA, the highest molecular weight, corresponding to $N = 527$, is around 83 kDa, while for PAA, $N = 500$ corresponds to $M = 36$ kDa, so the sample 527/500 in Fig. 10(a) is weakly entangled. For PDADMA/IBMA, the PDADMA molecular weight of 300 kDa is well above the entanglement threshold, and the dependence of the inverse crossover frequency on the molecular weight M of the polyanion IBMA shown in Fig. 12 (right) increases from quadratic to cubic as M increases beyond 100 kDa. This is a factor of 3–5 higher than one might expect from the above estimate $M_e \approx 10$ kDa, since the crossover should be at around two to three times M_e . In addition, the cubic dependence of relaxation time on chain length above M_e differs from the 5.4 power scaling observed for the PMAPTA/PMA discussed above. Thus, the estimated plateau moduli of the coacervates and the corresponding molecular weights at the transition to entanglement-dominated rheology are only very roughly consistent with theoretical expectations. The molecular-weight scaling of relaxation time and viscosity in the unentangled

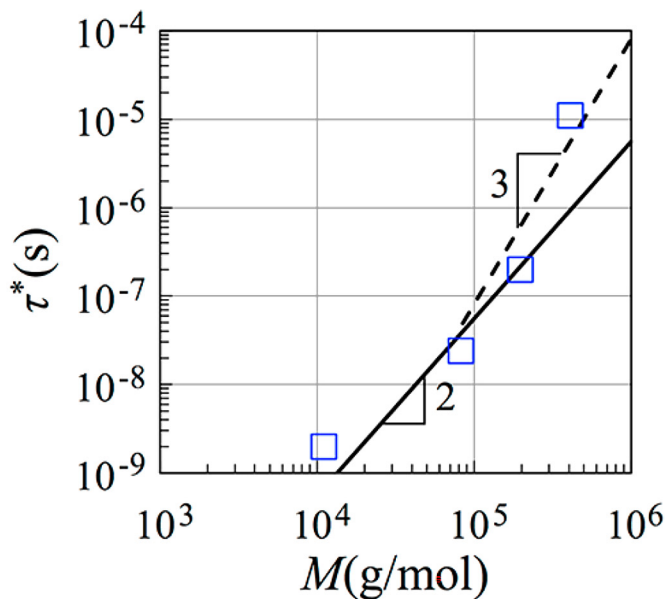
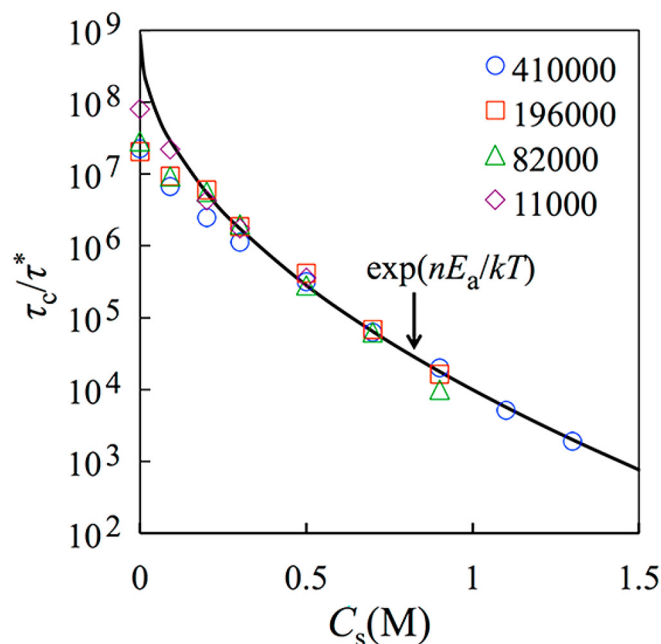


FIG. 12. (Left) Salt concentration dependence of relaxation time τ_c rescaled to a common curve by dividing τ_c by a molecular-weight-dependent time τ^* ; (right) the dependence of τ^* on polyanion molecular weight. τ_c is defined as the reciprocal of the crossover frequency at which $G' = G''$. The equation for the salt concentration dependence on the left is based on an activated process involving electrostatic interactions, as described by Hamad *et al.* [36]. Solid curves are based on Eqs. (4) and (5) with $n=5$, $1/\omega_0 = 10^{-12}$ s, and $d = 1.7$ Å. Used with permission from Hamad *et al.*, *Macromolecules* **51**, 5547–5555 (2018). Copyright 2018, American Chemical Society.

and entangled states are also roughly as expected, with the exception of PMAPTA/PMA, which shows much stronger molecular-weight scaling in the entangled state. (Note, that the monomer molecular weight of PDADMA is 126 Da and of IBMA is 170 Da, giving an average of 148 Da so that the number of monomers per entanglement is expected to be $N_e \approx 340$. PDMAEMA has a molecular weight of 157 Da and for PAA, it is 72 Da so that $N_e \approx 440$.)

VII. TIME- SALT-pH SUPERPOSITION

The work mentioned above was for strong PEs that remain nearly fully charged over a wide range of pH , or for weak PEs at pH values at which both PEs remain fully charged. However, Tekaat *et al.* [52] studied coacervates of PDADMA, a strong PE, and PAA, a weak one, under a range of pH values that led to partial neutralization, or protonation, of PAA. The molecular weights were relatively high, 100 000–200 000 Da for PDADMA and 100 000 Da for PAA, and the coacervate concentration resulting from phase separation seemed not to be reported. Titration curves allowed the charge level of the PAA to be determined as a function of pH and salt concentration, and coacervates were made with the concentration of PAA adjusted upward to compensate for the reduced charge level, to keep the number of PAA charges equal to the number of charges on the PDADMA as pH was varied. In the absence of salt, PAA became only half charged at a pH around 5.5, while much lower pH was required to achieve similar neutralization with added salt, a phenomenon known as “charge regulation.” Coacervates at the 1:1 charge ratio made from PDADMA and PAA at various pH values and at 0.25M KCl are shown in Fig. 13(a). It is noted in this figure that the G' and G'' curves shift to the left dramatically when the pH drops below 7, showing a counterintuitive *slowdown* in dynamics for *less-charged* PAA. Remarkably, Fig. 13(b) shows that curves at different pH can be superposed, primarily by shifting along the frequency axis, a phenomenon called “time- pH ” superposition, which holds for each salt concentration from 0 to 0.5M KCl. In addition, the time-salt superposition applies to these data as well, allowing a double superposition of data at all pH and salt concentrations into a “super-master” curve, shown in Fig. 14. The surprising slowdown in dynamics at reduced PAA charge at low pH in Fig. 13 is believed by Tekaat *et al.* [52] to be due to increased hydrophobic interactions between PAA chains made possible by the neutralization of charge. As we will see below, shifting of rheological curves due to hydrophobicity seems to correlate well with the concentration of water in the coacervate, but such a correlation cannot be checked for these data, since water concentrations were not reported by Tekaat *et al.* [52]. In fact, PAA at reduced pH can phase separate from water, depending on salt concentration and temperature [53]. This shows that interactions other than ionic can be important, and even dominate, the dynamics of coacervates.

VIII. TIME-HYDRATION SUPERPOSITION

Lutkenhaus and co-workers [54] recently explored the effect of hydration level on the linear rheology of poly(allylamine hydrochloride) (PAH) and poly(acrylic acid),

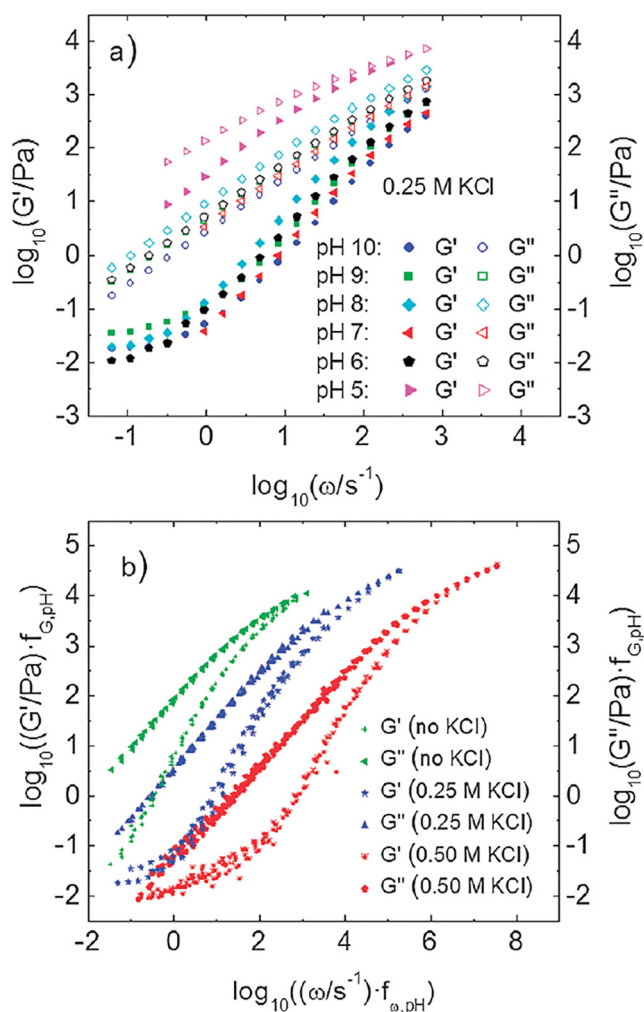


FIG. 13. (a) pH -dependent storage and loss moduli for PDADMA/PAA coacervates at pH values low enough that the PAA is no longer fully charged at a KCl concentration of 0.25M. (b) Master curves resulting from time- pH shifting primarily along the frequency axis but with a small vertical shift [52]. Used with permission from Tekaat *et al.*, Phys. Chem. Chem. Phys. **17**, 22552–22556 (2015). Copyright 2015, Royal Society of Chemistry.

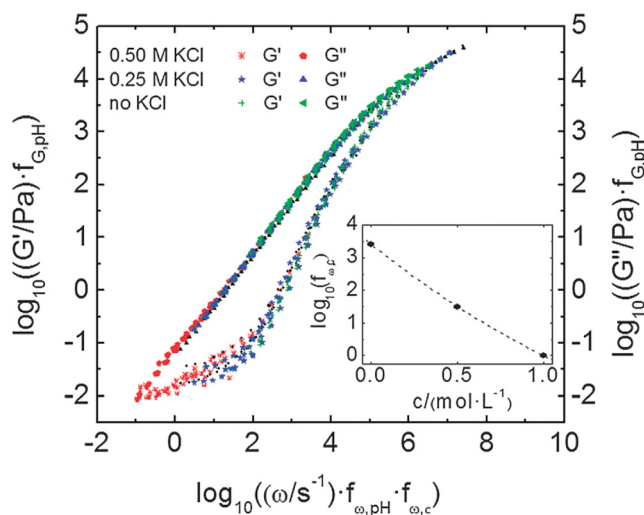


FIG. 14. “Super master” curve from shifting of master curves of Fig. 13(b). The inset shows the salt shift factor as a function of salt concentration [52]. Used with permission from Tekaat *et al.*, Phys. Chem. Chem. Phys. **17**, 22552–22556 (2015). Copyright 2015, Royal Society of Chemistry.

PAH/PAA, coacervates, where both PEs had molecular weights of around 100 kDa and found not only the time-temperature superposition but also the time-hydration superposition as the hydration level was varied from 13.5 to 35.7 wt. %. The superposition is shown in Fig. 15, for linear oscillatory extensional flow, yielding a dynamic Young's storage modulus E' . The hydration level was controlled through equilibration of samples at controlled relative humidity (RH) ranging from 50% to 95%, giving the above range of hydration levels. The temperature shift factor had an Arrhenius temperature dependence, with higher activation energies for higher levels of hydration. This is somewhat surprising since the sample relaxes faster at higher hydration. For RH between 80 and 95%, $E_a = 379 \pm 35$ kJ/mol, decreasing to 176 ± 20 kJ/mol for 70% RH, and down to 78 ± 57 kJ/mol for 50% RH. The logarithm of the shift factor for hydration, $\ln a_w$, was found to be linear in the weight percentage of water present. Thus, water acts as a strong "plasticizer" for the coacervate. The same group [55] found for the same PEs that the inverse "glass transition" temperature $1/T_g$ determined from scanning calorimetry depends linearly on the log of the number of water molecules per ion-pair, with data for different salt concentrations all collapsing onto a single curve. Other, thorough, work by this group, including detailed atomistic simulations for several PC/PA pairs, including PDADMA/PSS, have shown that water plays a central role in the local structure and dynamics of coacervates [13,56–58]. Connecting such findings to the rheological shift factors, and determining how the local structure controls those shift factors, should be a high priority for future work.

A likely similar hydration-controlled relaxation behavior was revealed when PE hydrophobicity was considered explicitly in studies by Shull and co-workers [59]. They quaternized poly(4-vinylpyridine) (QVP) polycations with methyl (QVP-C1), ethyl (QVP-C2), and propyl (QVP-C3) substituents, thus producing polycations with successively higher hydrophobicity but the same chain length and backbone

chemistry. These PEs had molecular weights of 60 kDa and coacervates were made of each of these with PSS, with 200–350 kDa. As expected, and shown in Fig. 16(a), the more hydrophobic PEs exhibited higher resistance to swelling with increased salt concentration. The swelling resulting from adding methyl groups onto the QVP side chains is not linear since the swelling curve for PSS: QVP-C3 differs more greatly from those for PSS: QVP-C1 and -C2 than these two differ from each other. Intriguingly, however, a crossplot of high-frequency modulus G_3^* versus swelling in Fig. 16(b) indicates that the effect of the hydrophobicity on the rheology is captured nearly completely by its effect on swelling with water since the modulus versus swelling curves for all three QVP substituents is the same. This seems to be the same phenomenon discussed in the paragraph above, where hydration level was controlled through RH, rather than by the hydrophobic groups on the polymer. The high-frequency modulus (in the MHz range) in these experiments by Sadman *et al.* [59] was measured in a quartz-crystal microbalance that simultaneously measured swelling as a function of salt concentration. The swelling for coacervates with PDADMA, a more hydrophilic PC, is much greater than for the QVP polycations [Fig. 16(a)], and the modulus versus swelling curve [Fig. 16(b)] deviates somewhat from the curves for the QVP monomers, indicating a lack of universality across all polycations. Sadman *et al.* [59] also examined the effects of various salts, including KBr, KCl, NaCl, LiCl, and CaCl_2 , on the swelling and the modulus, and again found a collapse of data when high-frequency modulus was plotted against swelling. The salt-dependent swelling increases in the order of the salts given above, which tracks their electronegativity and therefore their hydration. The high-frequency modulus is an indicator of "glassiness" of the coacervates, which in principle should be indicative of analogous shifts in lower-frequency rheology, but a precise connection has not been made, since complete rheological curves were not reported. It would be worth finding whether or not the change in salt identity (e.g., KBr, KCl, NaCl, LiCl, and CaCl_2) can be

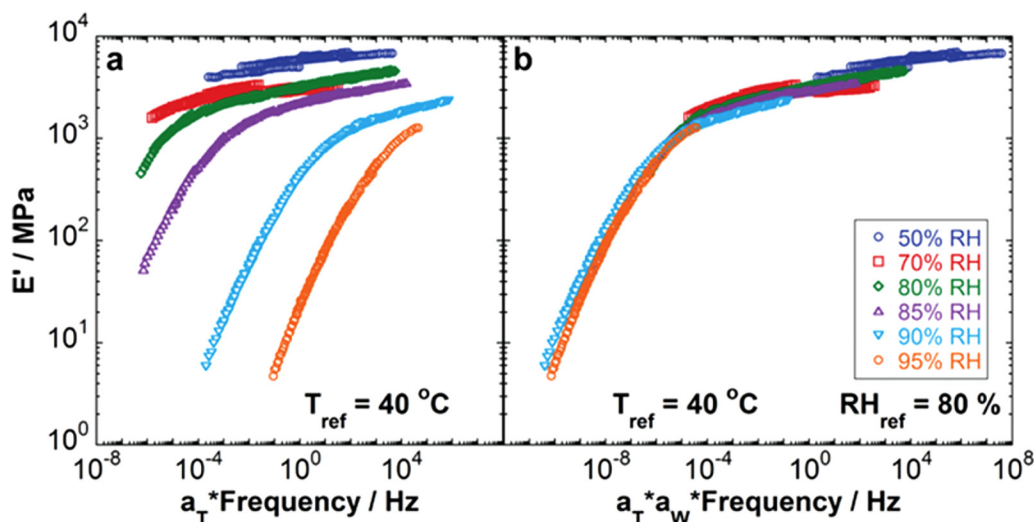


FIG. 15. (a) Time-temperature master curves of linear viscoelastic extensional storage modulus E' for RH of 50, 70, 80, 85, 90, and 95% from top to bottom. (b) Time-water "super master" curve from shifting curves in (a) with respect to the reference curve with 80% RH and $T_{ref} = 40$ °C [54]. Used with permission from Suarez-Martinez *et al.*, *Macromolecules* **52**, 3066–3074 (2019). Copyright 2019, American Chemical Society.

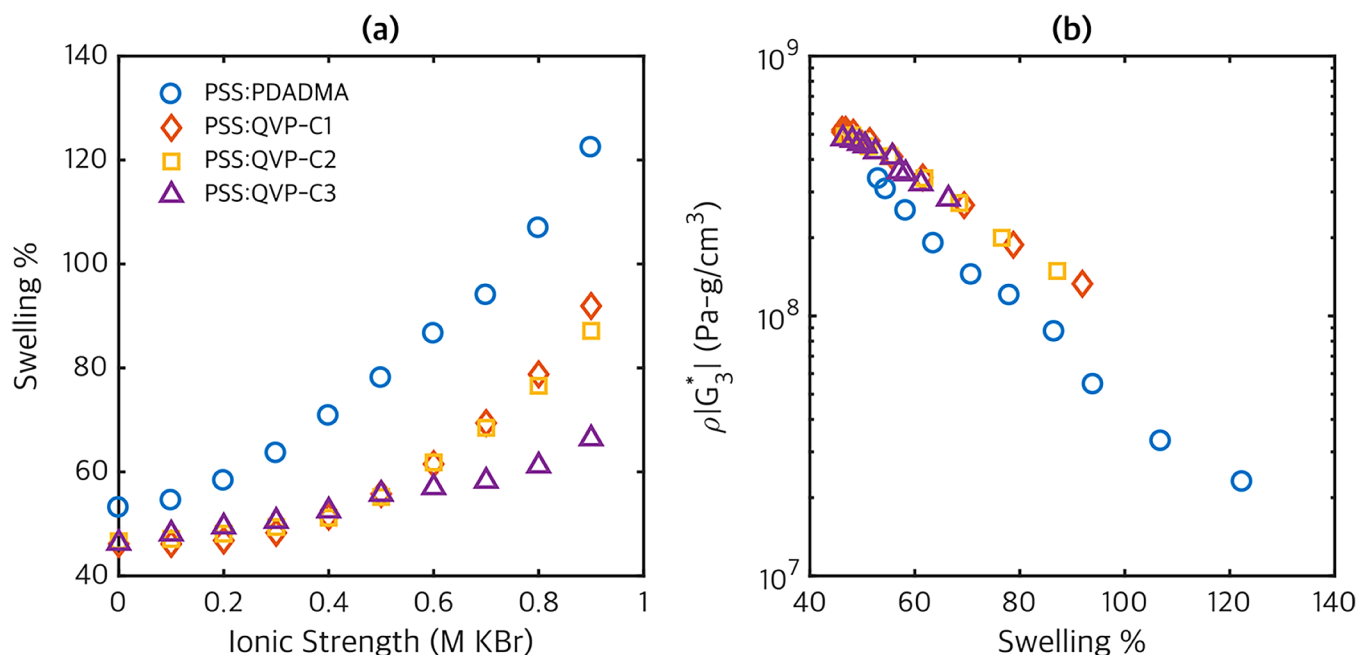


FIG. 16. (a) Swelling, i.e., water concentration as a percentage of polymer concentration, for PSS: QVP complexes, compared with that for PSS: PDADMA (blue symbols), as a function of KBr concentration measured by a quartz crystal microbalance (QCM). (b) Third-harmonic high-frequency complex modulus measured by QCM plotted against swelling [59]. Used with permission from Sadman *et al.*, *Macromolecules* **50**, 9417–9426 (2017). Copyright 2017, American Chemical Society.

encompassed in a master curve for all of these salt types. The indication that salt type and concentration exert their effects on rheology indirectly through their effects on water content is very much in line with an extensive body of work by Lutkenhaus [13], Sammalkorpi and co-workers referenced above, that reveals the key role of water in the local relaxation of coacervates.

Shull and co-workers [59] utilized the time-salt superposition with only horizontal shifts to obtain the master curves for each coacervate given in Fig. 17. The shift factors in the inserts to Fig. 17 show that the more hydrophobic PEs need higher salt concentrations to form the coacervates within the same modulus range, but once the salt concentration has been shifted, the rheological behaviors remain otherwise nearly independent of hydrophobicity. The curves can also be shifted onto a master curve when temperature is varied. Hence, these coacervates display “time-temperature-salt-hydrophobicity

superposition,” implying that temperature, salt, and hydrophobicity affect the rate of local monomer diffusion, but otherwise do not affect the long-range coacervate dynamics, which remains that of a simple viscoelastic liquid. The linear rheology is described by a simple expression for the complex modulus, namely,

$$\frac{G^*}{G^s} = \frac{(i\omega\tau)^\beta}{1 + (i\omega\tau)^{\beta-1}}, \quad (2)$$

with G^s being a high-frequency modulus, τ being the relaxation time, and β being a parameter around 0.42–0.44.

Hydrophobicity thus can have an effect on coacervate rheology; however, the importance of the effect seems to be system specific. Laaser and co-workers [60] also carried out systematic studies using nonionic monomers copolymerized

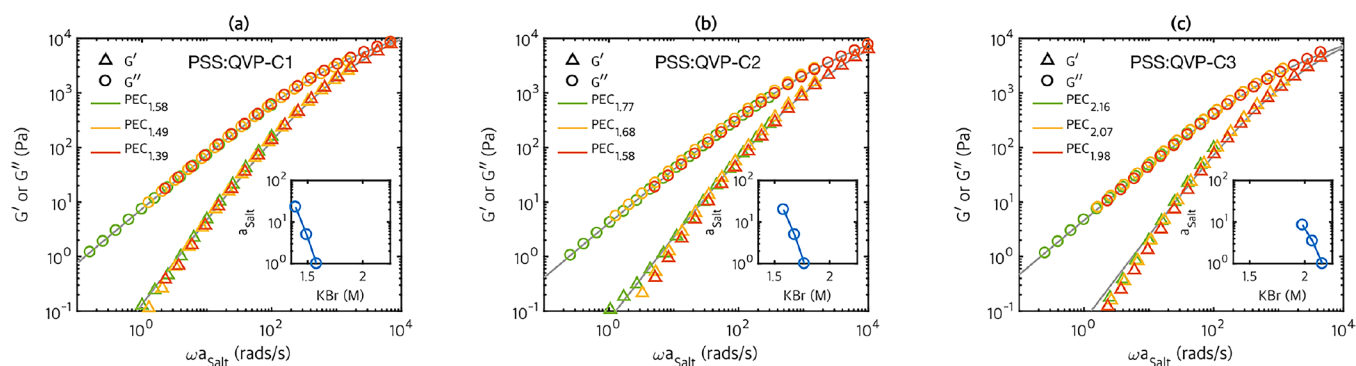


FIG. 17. Time-salt superposition with horizontal shifting only at 20 °C for (a) PSS: QVP-C1, (b) PSS: QVP-C2, and (c) PSS: QVP-C3. In the designation PEC_x in the legend, x is the molarity of KBr. Curves are shifted with respect to the highest salt concentration in each case [59]. Used with permission from Sadman *et al.*, *Macromolecules* **50**, 9417–9426 (2017). Copyright 2017, American Chemical Society.

with both polyanions and polycations in a series of acrylamide copolymers and saw a little effect of the hydrophobicity of the polyion on its rheological response. They speculated as to the cause of this lack of sensitivity, suggesting that an entropic effect may offset the effect of hydrophobicity.

Very recent work by the groups of Perry and Sing [51] also systematically explored the influence of hydrophobicity by comparing the phase behavior and rheology of the coacervates of two closely related pairs of polyions, namely a more hydrophobic methacryloyl-based polymer pair and a less hydrophobic acryloyl-based pair, where the backbones of all polymers are identical except that the former pair has an extra pendant methyl group. The former consisted of PTMAEMA with anionic PSPMA, while the latter acryloyl-based pair consisted of poly([2(acryloyloxy)ethyl]trimethylammonium) with poly(2-acrylamido-2-methyl-1-propanesulfonic acid). For the same degree of polymerization, the more hydrophobic pair showed a higher modulus and slower relaxation than the less hydrophobic pair, even at a higher salt concentration in the former, but most of this difference could be correlated with the polymer concentration, and thus the degree of hydration, which therefore again appears to be a critical parameter controlling the rheology.

Finally, we note that hydrophobic effects can be very complex. Meng *et al.* [3] found that coacervates made of poly(vinylbenzyl)trimethylammonium chloride (PVBTMAC) and PSS transitioned from a soft solid at zero salt with 90% water content to a stiff gel with lower water content at 2M NaBr, while transitioning back to a viscoelastic liquid at still higher NaBr. This unusual nonmonotonic dependence of stiffness on salt concentration was investigated by X-ray scattering and traced to the formation of hydrophobic domains that opened up upon increase in salt concentration, eventually evolving into a viscoelastic structure perhaps more similar to that of more typical coacervates. These system-specific results dampen hopes for a completely universal theory of coacervate phase behavior and rheology, although theories that encompass important sets of coacervates seem feasible.

IX. LOW-FREQUENCY PLATEAU MODULUS

Note in Figs. 13 and 14 the appearance of a *low-frequency plateau* in the storage modulus G' . This plateau, with a very low modulus of around 10^{-2} Pa, might suggest a transition to a solidlike gel, rather than fluid, at the lowest frequencies for this coacervate. However, even at the lowest frequencies we see that $G'' > G'$, implying that the response is still predominantly viscous. If the plateau is maintained to arbitrarily low frequency, eventually G'' would drop below G' and the sample would then be characterized as a very soft solid. Note that at zero salt concentration, there is no sign of a plateau, presumably because the frequency was not made low enough. It is also possible that such a low-frequency plateau would be found in other coacervates discussed thus far, if lower frequencies were accessed. Most such data in these figures do not reach G' values as low as 10^{-1} , let alone 10^{-2} Pa. (However, the data in Fig. 11 do show storage moduli this low with little sign of a plateau.) Data for PDMAEMA/PAA by Spruijt *et al.* in Fig. 5(e) [18] show an indication of a leveling off of G' at

the lowest frequencies, with G' around 10^{-1} or so. (Note the normalization of G' on the y axis of this plot.) A low-frequency plateau in G' of magnitude between 1 and 10 Pa was also observed in the time-ionic-strength shift factor data of Syed and Srivastava [50]. A weak low-frequency plateau in G' appears in data for coacervates of (poly)-lysine (PLK) and (poly)-glutamic acid (PRE) of Tirrell and co-workers [27] again with $G'' > G'$. These workers note the possibility that this weak “elastic” terminal response might be a rheological artifact given the weak stress level. Artifacts capable of producing a spurious low-frequency plateau of low magnitude include transducer torque or calibration limits, heterogeneities or low-concentration “gels,” impurities, or high-molecular weight tails in the samples, and “skin” formation on the edge of the rheometer sample due to evaporation.

A much more compelling demonstration of a transition to a solidlike rheological response at low frequencies is found in the studies of Perry and co-workers [61] for a coacervate of PDADMA with the molecular weight of $M_w = 289,100$ Da, $M_w/M_n = 1.3$ and PSS with $M_w = 354,400$ Da, $M_w/M_n = 1.7$ in KBr salt. The concentration of polymer in the coacervate varies with salt but is within the range 0.8 to 1.1M, which corresponds to volume fraction around $\phi \approx 0.125$ –0.17. Figure 18(a) shows that within the range 1.0–1.6M KBr, the time-salt superposition allows the production of a fluidlike master curve similar to that expected for unentangled solutions with near-terminal response at low frequencies. The lack of a clear terminal $G' \propto \omega^2$ behavior may owe to the high polydispersity of the samples. The horizontal and vertical shift factors are plotted in Fig. 18 against (b) polymer concentration and against, (c) overall salt concentration, and (d) salt concentration in the coacervate, which is much lower than the overall salt concentration due to strong partitioning of salt into the supernatant. When the overall salt concentration drops below 1M, however, Fig. 19 shows that the rheology changes to a low-frequency power-law scaling of both G' and G'' with $\omega^{0.3}$, which is “quasi-solidlike” since the exponent for G' is closer to zero (characteristic of a solid) than to 2 (characteristic of a liquid). Note the very large variation of shift factors with salt concentration, especially in Fig. 18, including a shift of more than two decades in the vertical shift factor, which is unusually high for vertical shifting. The results are suggestive of a more gradual shift to solidlike rheology below a critical salt concentration.

While the rheological transition to “solidlike” behavior reported above for PDADMA/PSS in KBr seemed to occur abruptly at a particular salt concentration, this transition was revealed to be continuous in the later work of Ali and Prabhu [62]. Figure 20 shows the time-temperature-salt superposed G' and G'' curves for PDADMA/PSS coacervates in both NaCl [Fig. 20(a)] and KBr [Fig. 20(b)]. Each curve in these figures is itself the result of a time-temperature (t-T) superposition, allowing data to be gathered over some 5–7 decades of frequency at each salt concentration. Achieving a large range of frequencies at each salt concentration is important in revealing the low-frequency break-down in time-salt (t-s) superposition. Notice that at high *reduced* frequencies, in the range 10^2 rad/s – 10^4 rad/s in Fig. 20, little deviation can be seen in t-s superposition, but that the deviation becomes

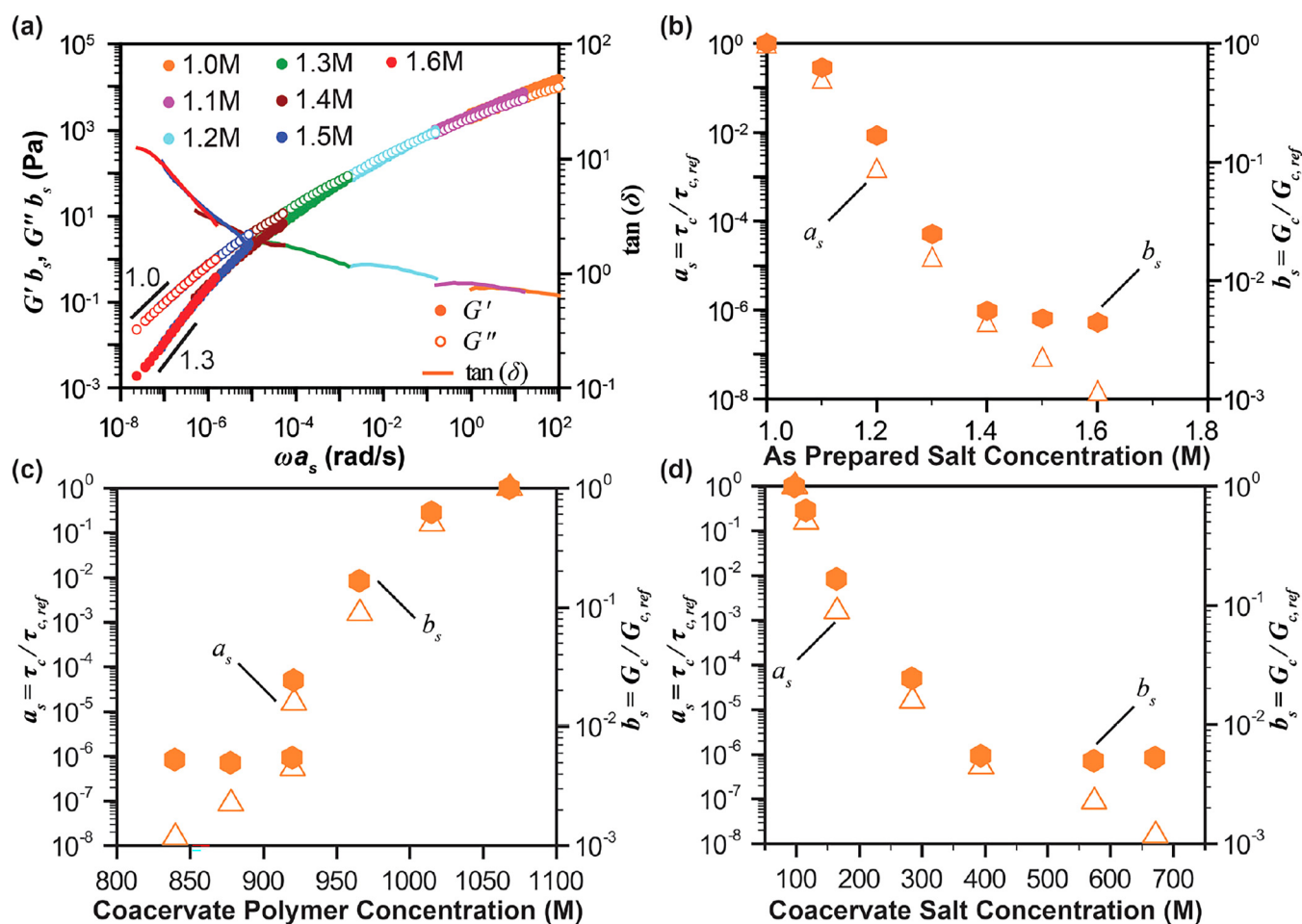


FIG. 18. (a) Time-salt superposed curves for PDADMA/PSS (with from 1.0 to 1.6M KBr), where the given salt concentrations were as prepared in the initial mixture prior to phase separation. (b) horizontal (open triangles) and vertical (solid hexagons) shift factors, a_s and b_s , as a function of the “as prepared” salt concentration. The same shift factors are also plotted with respect to the (c) measured polymer concentration and (d) measured salt concentration, both in the coacervate phase. Note that the monomer and salt concentrations in the lower figures should be in units of millimolar, mM, not molar M [61]. Used with permission from Liu *et al.* *Soft Matter* **13**, 7332–7340 (2017). Copyright 2017, Royal Society of Chemistry.

huge at lower frequencies. In Fig. 18(a), on the other hand, also for PDADMA/PSS, the data were taken at a single temperature and data at each salt concentration extended only over two decades. Thus, the data at different salt concentrations barely overlap in Fig. 18(a). Hence, the “superposition” shown in Fig. 18(a) is evidently only apparent, made possible by shifting both vertically and horizontally and allowing curves to be stitched together despite lacking true t-s superposition. Notice the discontinuities evident in the $\tan \delta$ curves, where data for different salt concentrations are forced to meet up. Even more telling is the very large vertical shift factors in Fig. 18(b), which are much larger than is typical in most superpositions. They are also much larger than those shown in the inset of Fig. 20(b), for a nearly identical system, differing only in that the molecular weights of PDADMAB (PDADMA with bromide ion) and KPSS (PSS with potassium ion) are 150 and 200 kDa, respectively, in Fig. 20 from the work of Ali and Prabhu [62], while they are 289 and 354 kDa in the work of Liu *et al.* [61] in Fig. 18. The vertical superpositions in the insets in Fig. 20 are more modest than in Fig. 18, because in Fig. 20 curves at different salt concentrations are not forced to superpose except at high

frequency. Thus, Fig. 20 suggests that t-s superposition should be carried out only when a wide enough frequency range (at least 4 decades) is covered at each salt concentration, ideally obtained by carrying out the t-T superposition prior to t-s superposition, or where this is lacking, using a wide range of frequencies at a single temperature. Figures 2 and 6 of Schlenoff *et al.* show cases in which wide ranges of frequencies at each salt concentration are obtained by the t-T superposition. While some nonoverlapping data at low frequencies in Fig. 6 indicates some deviation from t-s superposition, any transition to a plateau in G' at low frequency is very weak at best in these data, even for virtually zero salt concentration.

Thus, the transition from a liquidlike terminal region to a solidlike plateau at low frequency appears to be a nonuniversal feature of only some coacervates, and when it occurs, does so at low salt concentration. Salt, then, can play two roles; it can both act to speed up “sticky diffusion” of the polymer by acting to “plasticize” the ion-pairing, and it can act to break up an otherwise permanent gel-like structure that is manifested at low frequency. The latter role, since it emerges at low frequency, presumably acts on longer length scales than do individual ion pairs and their spacing. The modulus that emerges

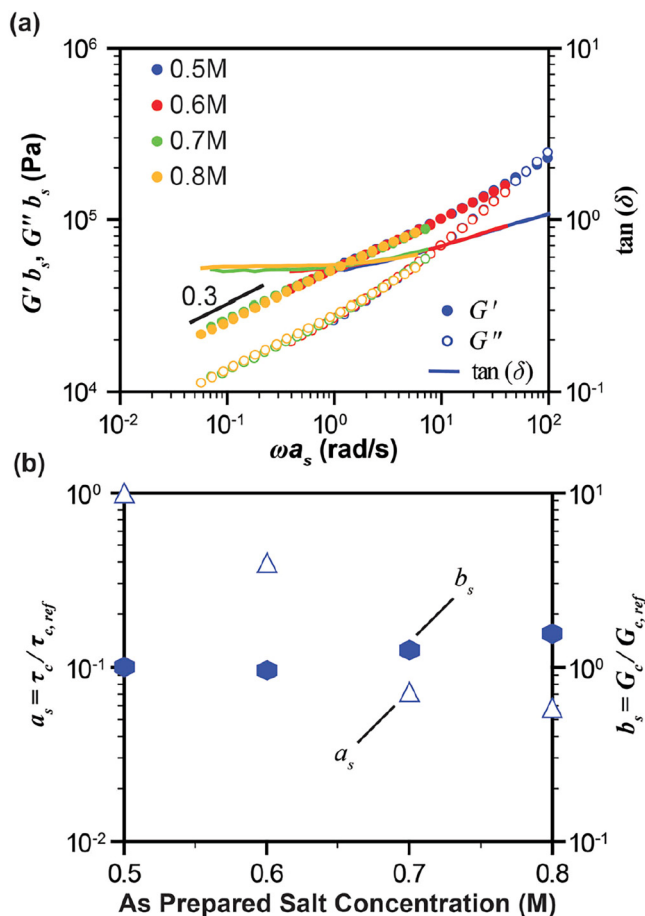


FIG. 19. (a) Similar to Fig. 18, except for lower salt concentrations (from 0.5 to 0.8M KBr). (b) Plot of the horizontal (open triangles) and vertical (solid hexagons) shift factors, a_s and b_s , as functions of the “as prepared” salt concentration [61]. Used with permission from Liu *et al.* *Soft Matter* **13**, 7332–7340 (2017). Copyright 2017, Royal Society of Chemistry.

at low frequency and low salt is as high as 10^2 Pa, which, though higher than observed in Fig. 14, nevertheless, using Eq. (1), suggests a polymer network strand size much larger than the molecular weights of the polymers themselves. However, the data in Fig. 20 (left) are for NaCl concentrations of 2.8M or higher. Shamoun *et al.* [63] also carried out rheological experiments with PDADMA/PSS in NaCl, with roughly similar molecular weights, i.e., 400 kDa / 200 kDa, as the values used to obtain Fig. 20, which are 150 kDa / 200 kDa. Shamoun *et al.* [63] accessed a lower salt range, and observed a much higher low-frequency plateau, one that decreased from 3×10^4 to 1.5×10^4 Pa over the range $[\text{NaCl}] = 0.1\text{--}1.0\text{M}$. The results at 1.0M are shown in Fig. 21. These low-frequency moduli are around 2 decades higher than for the Ali-Prabhu data at 2.8M NaCl in Fig. 20. Thus, putting these two studies together, it appears that the low-frequency plateau is sensitive to salt concentration, becoming much higher with decreased salt concentration. Note also in Fig. 20 the strong influence of the salt type on the salt concentration at which the transition from liquidlike to solidlike behavior occurs. It is possibly significant that all of the PE pairs showing a low-frequency plateau in G' have been of rather high molecular weight, over 100 kDa up to 400 kDa. Whether the plateau is molecular-weight sensitive, as well as salt-type and salt-concentration sensitive is an interesting question. Some possible reasons for the formation of a low-frequency “gel-like” structure will be suggested in the theory section. For low concentrations of salt, Fig. 21 shows that PDADMA/PSS exhibits an interesting transition at high frequency to a “glassy” modulus of 10^7 Pa [63]. This “glassy” modulus remains, however, much lower (by more than an order of magnitude) than the modulus of dense (solvent-free) polymer glasses, and does not show the relatively sharp enthalpy

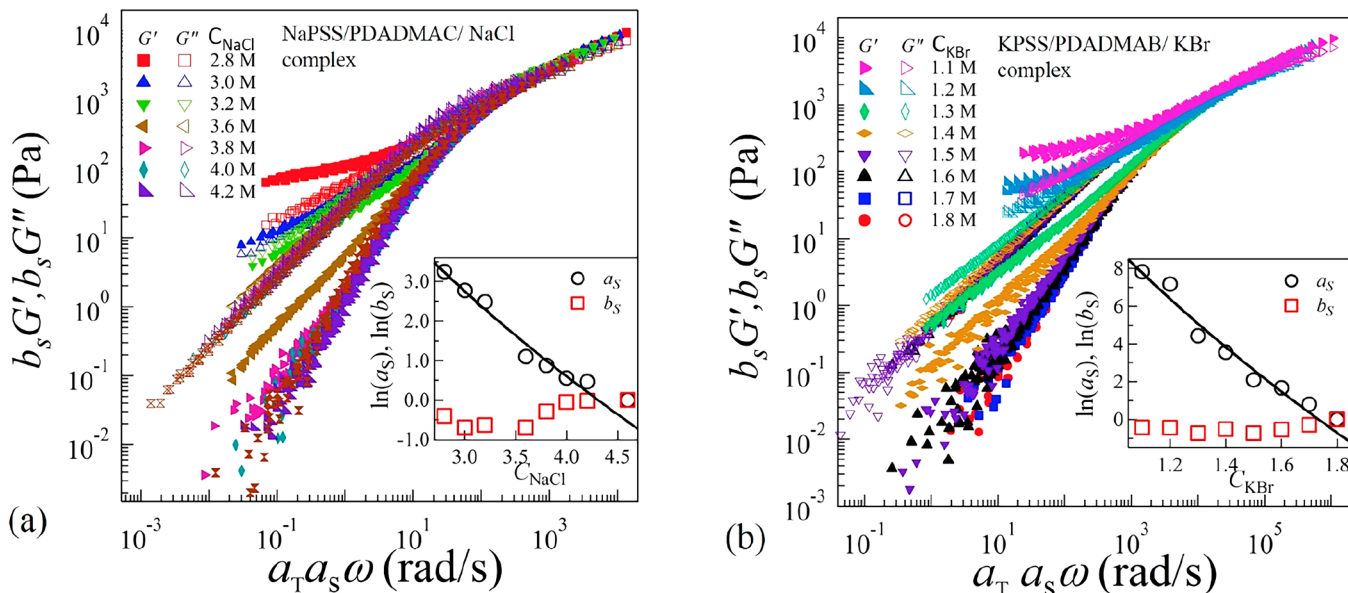


FIG. 20. Time-temperature-salt superposition curves for coacervates composed of PDADMA/PSS in (a) NaCl, shifted relative to the curve at $[\text{NaCl}] = 4.6\text{M}$ and (b) KBr, shifted to $[\text{KBr}] = 1.8\text{M}$. Insets show horizontal a_s and vertical b_s shift factors [62]. Used with permission from Ali *et al.*, *Gels* **4**(1), 11 (2018).

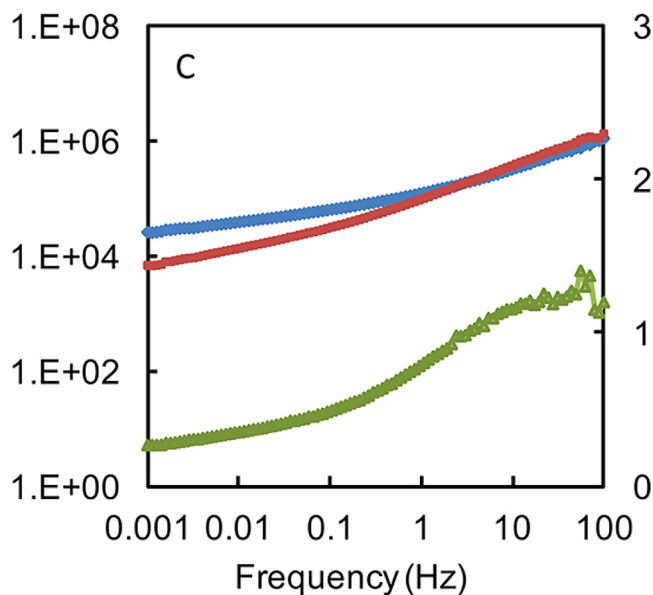


FIG. 21. G' (blue \blacklozenge , upper), G'' (red \blacksquare , middle) in units of Pa, and loss $\tan(\delta)$ (green \blacktriangle , lower) for PDADMA/PSS coacervate with 1.0M NaCl at 30 °C [63]. Used with permission from Shamoun *et al.*, *Macromolecules* **45**, 9759–9767 (2012). Copyright 2012, American Chemical Society.

change with temperature upon cooling into the “PE glass.” While of considerable interest in its own right, this “glassy” behavior is not the focus of this article, and readers interested in this behavior are referred to work by Lutkenhaus *et al.* among others [13]

X. THEORY

Starting with Spruijt *et al.* [17,18] the rheological behavior of coacervates has generally been interpreted using the “sticky diffusion” theory of Rubinstein and Semenov [2]. The idea is that monomers on different chains form temporary attractive bonds whose rate of breakage or formation (which are equal at equilibrium) sets the time scale τ_0 for local diffusive motions. Longer-range motions are then identical to that of ordinary polymers, except that all time scales of polymeric relaxation are proportional to this fundamental “stickiness time scale” τ_0 . For unentangled polymers, the dynamics are then those of Rouse polymers, with a set of relaxation times given by

$$\tau_p \approx \tau_0 (f/p)^2; \quad 1 < p < f; \quad \tau_R = \tau_0 f^2, \quad (3)$$

where f is the number of stickers on the chain and p is the “mode number,” which is smaller for the longer relaxation times. The first mode, with relaxation time $\tau_1 = \tau_R$ represents the relaxation of the entire chain, while the higher modes, with $p > 1$, describe a series of harmonics of the primary mode. Modes with higher p represent more localized, and, therefore, faster, relaxations along the chain. Each relaxation time, including the longest, with $p = 1$, and $\tau_R \propto f^2$, depends quadratically on the number of stickers f per chain. If the chains become long enough to exceed their entanglement threshold, the sticky diffusion model predicts that the longest relaxation time should transition to that of reptation, characterized by the

tube disengagement (or reptation) time, which scales as $\tau_d \propto f^3$. These formulas assume that the sticker strength is high enough, and, therefore, τ_0 is long enough, that sticker breakage time controls the chain relaxation rate, rather than ordinary frictional contacts between chains. For a coacervate containing PEs of opposite charge, the “stickers” can be interpreted as charged monomers that bind ion pairs of the opposite charge. If all, or a fixed fraction, of monomers are charged, then the longest relaxation time scales with molecular weight M as $\tau_R \propto M^2$ and $\tau_d \propto M^{3.4}$, which are the same scaling laws as found for neutral polymers in the unentangled, and entangled, limits, respectively. The corresponding scaling laws for the zero-shear viscosity are $\eta_0 \propto M$ and $\eta_0 \propto M^{3.4}$, respectively. In addition, the sticky diffusion theory predicts that the relaxation modes in both limits are the same as for neutral polymers, with only their overall magnitude, set by τ_0 , reflecting the influence of electrostatic interactions.

Thus, if sticky diffusion describes the rheology of coacervates, one expects the linear rheology, reflected in the shapes of the G' and G'' curves, to look essentially the same as for neutral polymers. In addition, there should be a transition, with increasing chain length, from a shape similar to that of the Rouse theory for unentangled chains, to that of the Doi–Edwards theory for entangled chains. A transition from Rouse-like G' and G'' curves to shapes consistent with the onset of entanglements can be seen in Fig. 6, as the number of monomers increases from $n_{av} = 213$ to 2097, and in Fig. 5, as it increases from around 20 to 500. Curves of similar shape can be found for neutral polymers as the molecular weight increases [47]. However, as noted earlier, Fig. 9 shows a viscosity scaling law of $\eta_0 \propto M^{3.4}$ for PMAPTA/PMA PEC, which is not explained by any simple local version of the sticky diffusion theory. Schlenoff and co-workers suggest a mechanism to explain this scaling based on frequencies of breaking of ion pairing that are correlated to allow a chain to slide through an entanglement [43]. In addition to the anomalous molecular weight scaling of the longest relaxation time, the shapes of the G' and G'' curves are more “smeared out,” with less distinctive features, and less clear-cut scaling laws in the low-frequency regime, than for neutral polymers of similar polydispersity. This again suggests that the dynamics and rheology of at least some PECs are not identical to those of melts apart from a stickiness lifetime taking the place of a monomeric friction coefficient. There are also anomalies in the emergence of low-frequency plateaus revealed in Figs. 13, 14, 19, and 20, which seem to be as-yet unexplained aspects of the rheology of coacervates.

For datasets that lack these anomalies, such as those of Figs. 5 and 6, ordinary polymer theories (Rouse and reptation) explain at least qualitatively both the frequency dependencies and molecular weight dependencies of the moduli. This leaves to be explained only the dependences of the fundamental time constant τ_0 on salt concentration, temperature, polymer concentration, and pH (for weak PEs). Of these, the most interesting and distinctive of PEs, is the dependence on salt concentration.

A general expression for the ion-pair breakage time τ_0 based on an “activation energy” E_a for bond breakage on salt concentration is

$$\tau_0 = \frac{1}{\omega_0} \exp\left(\frac{E_a(c_{salt})}{k_B T}\right), \quad (4)$$

where ω_0 is a fundamental ion-pair breakage attempt frequency (which is weakly temperature-dependent). The time-salt shift factor a_s is then obtained from the dependence of the time constant τ_0 on salt concentration, which arises from the salt-dependence of E_a . Significantly different expressions for $E_a(c_{salt})$ have been suggested. The first of these is due to Cohen Stuart and co-workers [17] who developed a model for local rearrangement of two pairs of oppositely charged monomers that exchange partners, as illustrated by the four charges in Fig. 4 [28]. To pull apart a pair of elementary opposite charges, each of charge magnitude e , in a dielectric medium with dielectric constant ϵ_r , from a contact separation d out to infinite distance, is simply the electrostatic energy ℓ_B/d . Here, $\ell_B = e^2/4\pi\epsilon_r\epsilon_0k_B T$ is the ‘‘Bjerrum length’’ involving the fundamental unit of charge of an electron, e , the dielectric constant ϵ_r (≈ 80 for pure water), and the dielectric permittivity in a vacuum ϵ_0 . The Bjerrum length is the length scale at which the electrostatic energy is comparable to thermal energy $k_B T$. However, when salt is present, the charge interactions are screened out at large distances. The simplest theory for screening is based on the linearized Debye–Hückel theory, in which the screening length, based on the salt ions only is the Debye length $\kappa^{-1} = \sqrt{1/(8\pi\ell_B N_{Av} c_{salt})}$, where N_{Av} is Avogadro’s number. Thus, electrostatic energy divided by $k_B T$ is cut off at the Debye length and the energy to pull the two charges apart is then $(\ell_B/d - \ell_B\kappa)$. Spruijt *et al.* [17,18] suggested that $n=2$ pairs of such charges must be separated in the transition state between the binding states on the right and left in Fig. 4, giving the transition energy as

$$\frac{E_a}{k_B T} = n\ell_B(1/d - \kappa) = n\ell_B\left(1/d - \sqrt{8\pi\ell_B N_{Av} c_{salt}}\right). \quad (5)$$

Taking $n=2$ pairs of charges and using Eq. (4), Eq. (5) can be written as

$$\ln(\tau_0\omega_0) = \frac{E_a}{k_B T} = -2\kappa\ell_B + \frac{2\ell_B}{d} = -A\sqrt{c_{salt}} + B. \quad (6)$$

The Debye length κ^{-1} decreases with the salt concentration as $1/\sqrt{c_{salt}}$, giving rise to the dependence shown in the third equality in Eq. (6), where $A = (32\pi N_{Av}\ell_B^3)^{1/2}$, $B = 2\ell_B/d$, and c_{salt} is in units moles/m³. (If the concentration units are moles/liter, a factor of 10^3 will need to multiply N_{Av} in the expression for A , as appears in some publications.) The same argument was made by Colby and co-workers, except they found their results were better fit with a transition state involving $n=5$ pairs of ions rather than 2 [36]. The derivation leading to Eq. (6) involves the Debye–Hückel far-field limit of electrostatic interactions, which is valid when charge interactions are weak, but can certainly be doubted when applied to ion-pairs, as discussed below.

Equation (6) can be used to predict the time-salt shift factor a_s used to shift the log frequency axis of a rheology

curve (such as G') relative to the curve at a reference salt concentration $c_{salt,ref}$. According to Eq. (6), such curves shift by a logarithmic amount $\ln \tau_0$ so that the time-salt shift factor, relative to the reference salt concentration, is given by

$$\ln a_s = -A(\sqrt{c_{salt}} - \sqrt{c_{salt,ref}}), \quad (7)$$

where $a_s = 1$ at $c_{salt} = c_{salt,ref}$. The predictions of Eq. (7) are compared in Fig. 22(a) to data for the shift factors from the rheological data of Spruijt *et al.* [18] in Fig. 5. Note in Fig. 22(a) that the logarithm of the shift factor seems to fit the square root dependence on salt concentration from Eq. (7) reasonably well but because of the limited range of salt concentrations a linear fit does almost as well. The curves shift significantly with different molecular weight, since the characteristic time τ_c is the inverse of the terminal crossover frequency extrapolated from zero frequency. From the rheological relaxation spectrum, Spruijt *et al.* estimated the lifetime of an ion pair to be around 200 ms at 0.6M salt, a value very much larger than estimated by Akkaoui *et al.* [43]. The latter give survival time of an ion pair to be around 10^{-8} s, and the hopping time for a broken pair to find a new pair rather than reforming the original pair to be around 10^{-4} s. These much shorter ion pair lifetimes of Akkaoui *et al.* are much more compatible with the sticky diffusion model, which gives Rouse terminal relaxation times that are a factor of f^2 times the ion-pair hopping time, as discussed in the theory section. The expression for the modulus near the terminal relaxation, which is given by $G \approx k_B T \phi_p f / N b^3$, allows the estimate $f \approx 100 - 1000$ for the data of Spruijt *et al.* for degree of polymerization $N \approx 500$.

The shift factor formula of Spruijt *et al.*, Eq. (7), seems successful for shifting their data for coacervates of PDMAEMA/PAA in NaCl and has also been successfully used by Ali and Prabhu [62] with $A = 6.8 \pm 0.6$ and 23.8 ± 2.5 for their time-salt shift factors a_s for PDADMA/PSS coacervates in NaCl and KBr, respectively. The prefactor A obtained from the fit by Ali and Prabhu is in reasonable agreement with the value calculated from the formula above using the expected value of $\epsilon_r = 42$ at the reference salt concentration if we take $n=1$ and $n=4$, respectively for NaCl and KBr salts. Meng and Tirrell [3] also report that changes in $\ln a_s$ are proportional to $-\sqrt{c_{salt}}$, in agreement with the scaling in Eq. (6). Hamad *et al.* [36] found the same scaling behavior for PDADMA/IBMA/NaCl, giving a plot of $\ln a_s$ against $-\sqrt{c_{salt}}$ very similar to that of Spruijt *et al.* shown in Fig. 22(a). As noted earlier, however, Hamad *et al.* found a best fit to the theory in Eq. (6) by modifying the factor of 2 in Eq. (6) to 5 pairs of ions broken in the transition state. This may suggest conformational restrictions that require a few, rather than 2, ion pairs to be broken to allow repairing of the freed charged monomers. Thus, a significant body of work is consistent with a scaling law $\ln a_s \propto -\sqrt{c_{salt}} + \text{const.}$, as shown in Table II. We note that Syed and Srivastava [50] varied the total small-ion ionic strength I , and found that the time-salt master curve was a universal function of total ionic strength I for PAH/PAA coacervates, with a constant, $A = 4.74$, in Eq. (6), with ‘‘T’’

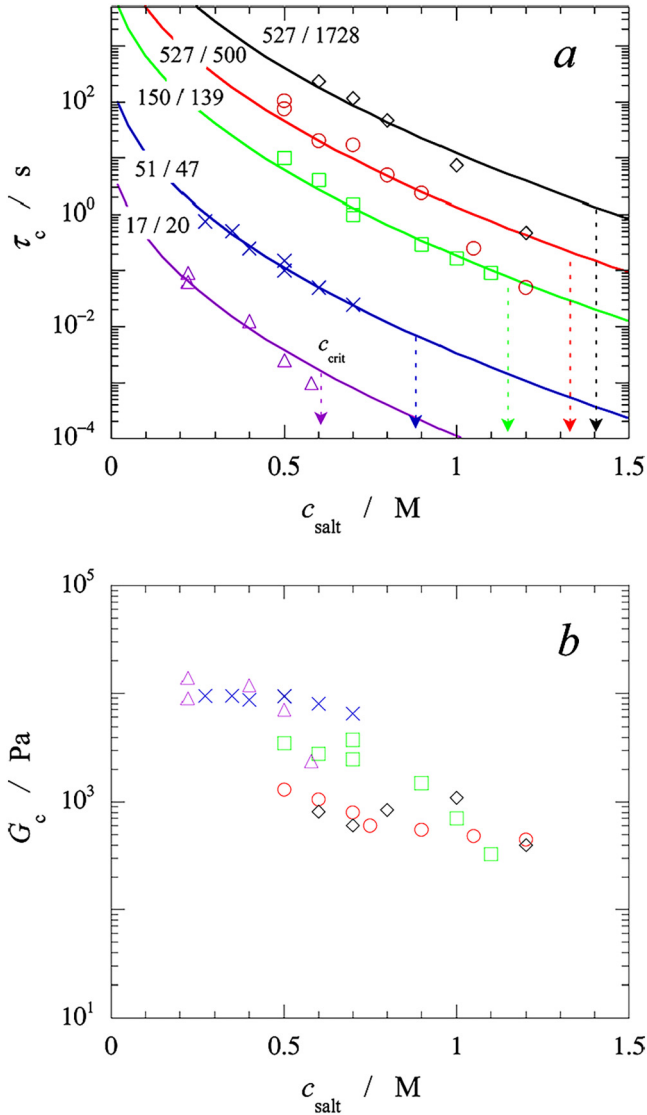


FIG. 22. Symbols show (a) horizontal and (b) vertical shift factors used to obtain master plots in Fig. 5 for PDMAEMA/PAA coacervates with the degree of polymerization indicated by matching colors (or shades in black and white) in (a) and (b) with fits in (a) given by Eqs. (4) and (5). The vertical dashed arrows in (a) indicate the critical salt concentrations for the dissolution of coacervate for each chain length [18]. Used with permission from Spruijt *et al.*, *Macromolecules* **46**, 1633–1641 (2013). Copyright 2013, American Chemical Society.

replacing “[NaCl],” which they interpreted as support for the sticky diffusion model of Spruijt *et al.* [18].

However, not all available papers show this behavior. A linear dependence, $\ln a_s \propto -c_{\text{salt}} + \text{const.}$ has been reported both by Sadman *et al.* [59] for coacervates of QVP/PSS in KBr solutions, and by Marciel *et al.* [27] for PLK/PRE in NaCl solution. In both cases, this dependence was simply reported as an empirical observation; no theory supporting this scaling has yet been offered. A slight variation from this dependence, namely $\ln a_s \propto -(c_{\text{salt}})^{6/5} + \text{const.}$ was observed by Shamoun *et al.* [63]. These different observed formulas for salt shifting are given in Table II.

Even where data is well fit by $\ln a_s \propto -\sqrt{c_{\text{salt}}} + \text{const.}$, there is reason to doubt the theory based on the Debye–Hückel approximation, which is a low-salt theory that treats ions as if they are in a diffuse double layer. Not only is the

diffuse double layer assumption highly questionable under typical (high) salt concentrations, and high charged monomer concentrations of around 1M, but the theoretical expression in Eq. (6) suggests that all monovalent salt ions should give the same shift factors, and indeed, even the same G' and G'' for the same polymers in different salt solutions. Figure 20, however, shows that this is definitely not true, since the rheology of the same PDADMA/PSS polymers differs greatly between NaCl and KBr solutions. Schlenoff and co-workers have found strong salt-type dependences of phase behavior of coacervates [64], and the same sensitivity should carry over to rheology. Also, if movement of a monomer requires breaking n ion pairs, then the coefficient of $\sqrt{c_{\text{salt}}}$ is $A = n(8\pi 10^3 N_A v \ell_B^3)^{1/2} = 5.8n$, if $\epsilon_r = 42$ (or $2.2n$, if $\epsilon_r = 80$) where the factor of 10^3 enters because we use molar units for the salt concentration rather than moles/m³. Thus, each increase in $\sqrt{c_{\text{salt}}}$ by one unit of square root molar concentration increases the shift factor by $5.8n$, and matching the time-salt shift factor in Fig. 22(a) implies that $n \approx 2$. Similarly, data from supplementary information in Akkaoui *et al.* [43] show a fivefold change in a_s with a change in NaCl concentration from 0 to 0.2M, again implying that $n \approx 2$, if we use Eq. (6).

Thus, some support of Eq. (6) might be drawn from the agreement of the fitted value of the prefactor A with the predicted value when we take $n \approx 2$. However, as noted above, the number n of ion pairs broken during each rearrangement step has been adjusted by Hamad *et al.* [36] to make the calculated A agree with the fitted one, and so support for Eq. (6) from this direction is shaky. In fact, the expression for τ_0 in Eq. (6) depends on temperature as well as salt concentration, through the dependence of $\ell_B = e^2/4\pi\epsilon_r\epsilon_0 k_B T$ on temperature and a weaker dependence of the prefactor ω_0 on temperature. If the salt concentration is zero, then the temperature-dependent shift factor a_T is given by the temperature dependence of $B = n\ell_B/d = ne^2/4\pi d\epsilon_r\epsilon_0 k_B T = 1.4 \times 10^{-4} n/d\epsilon_r RT$, in mks units, using the known values of e and ϵ_0 and switching to molarity rather than molecular units. If the binding distance d is around 1 nm, and ϵ_r around 44, then $B = 3.1n \text{ kJ/mol}/RT$, with RT in KJ/mole. This corresponds to Arrhenius time-temperature shifting with an activation energy of $3.1n \text{ kJ/mol}$. However, the activation energy for time-temperature shifting for PMAPTA/PMA coacervates at near-zero salt concentration reported by Akkaoui *et al.* [43] is 45 kJ/mol, which would require an unreasonable 15 pairs of ions to break for local chain motion to occur. Admittedly, some of the temperature dependence is likely owing to the temperature dependence of the viscosity of water, which can be approximated at around room temperature as the Arrhenius with the activation energy of around 23 kJ/mol. If the rate constant ω_0 in Eq. (5) is inversely proportional to the viscosity, this still leaves an electrostatic activation energy of 22 kJ/mol, requiring around 7 pairs of ions to be broken to explain the temperature dependent shift factor. Moreover, since this number n must be the same value for both the salt-dependent and temperature-dependent shifting, and the value needed for salt-shifting noted above is close to 2, much lower than the value of 15 (or possibly 7) needed for temperature shifting, expression (6) appears to make

TABLE II. The literature on time-salt/ ρ H/hydration superposition of coacervates.

Reference	Polycation/polyanion	Salt	Superposition ^a	t-T fitting form	Low- ω plateau?	Salt shift-factor fitting ^b
[18]	PDMAEMA/PAA	KCl	t-s	—	No	$\ln a_s = B - A\sqrt{c_{salt}}$
[36]	PDADMA/IBMA	NaCl	t-s	—	No	$\ln a_s = B - A\sqrt{c_{salt}}$
[62]	PDADMA/PSS	NaCl, KBr	t-T-s	WLF	Yes	$\ln a_s = B - A\sqrt{c_{salt}}$
[63]	PDADMA/PSS	NaCl	t-T-s	WLF	Yes	$\ln a_s = B - A(c_{salt})^{6/5}$
[3]	PVBTMA/PSS	NaBr	t-s	—	No	$\ln a_s = B - A\sqrt{c_{salt}}$
[59]	PVP/PSS	KBr	t-s	—	No	$\ln a_s = B - Ac_{salt}$
[27]	PLK/PRE	NaCl	t-s	—	Yes	$\ln a_s = B - Ac_{salt}$
[28]	PMAPTA/PMA	NaCl	t-T-s	Arrhenius	No	$a_s = a_{s,\tau_p} a_{s,f} a_{s,\varphi} a_{s,d} a_{s,N_e}$
[43]	PMAPTA/PMA	NaCl	t-T-s	Arrhenius	No	$a_s = a_{s,\tau_p} a_{s,f} a_{s,\varphi} a_{s,d} a_{s,N_e}$
[54]	PAH/PAA	NaCl	t-T-water	Arrhenius	No	$\ln a_w = B - AW_{H_2O}$ ^c
[50]	PAH/PAA	NaCl	t-s-ionic strength	—	Yes	$\ln a_s = B - A\sqrt{c_{salt}}$
[52]	PDADMA/PAA	KCl	t- ρ H-s	—	Yes	—(no relevant equation)

^a“t-T-s” represents time-temperature-salt superposition; “t- ρ H-s” represents time- ρ H-salt superposition; “t-T-water” represent time-temperature-water superposition; “t-s-ionic strength” represents time-salt-ionic strength superposition.

^bUnits of c_{salt} in the table are mol/m³ (1 mol/m³ = 10³ mol/l = 10³ M).

^c a_w , water shift factor; W_{H_2O} , water content in the PEC.

temperature-dependent and salt-dependent shifting incompatible. In addition, Eq. (6) depends on a theory of coacervation controlled by Debye–Hückel electrostatic fluctuations. The original Overbeek–Voorn theory [44] for the thermodynamics of coacervation assumed that these electrostatic interactions dominate, but recent evidence strongly points toward ion-specific binding as at least as important a factor for typical coacervate concentrations [64,65]. If thermodynamics of coacervation is not governed predominantly by Debye–Hückel electrostatics, neither should one expect such electrostatics to govern the rheology.

Perhaps, the most telling argument against the scaling $\ln a_s \propto -\sqrt{c_{salt}} + \text{const.}$ is simply that this dependence of $\ln a_s$ on the square root of salt concentration does not fit any of the datasets significantly better than does a simpler linear fit, $\ln a_s \propto -c_{salt} + \text{const.}$, and for some of the datasets in Table II, the square root rule is significantly worse. This is demonstrated in the SI [69], where all datasets discussed in Table II are fit by both square root and linear scaling rules using linear regression, and the goodness of fits, measured by the statistical values of R^2 , are compared. Like many of the others, the datasets of Spruijt *et al.*, have such a modest range of salt concentration that both scaling laws fit the data with an R^2 value of 0.96–0.99, with each scaling law showing a better agreement for a portion of the datasets. For some of the datasets of Marciel *et al.* [27] and Hamad *et al.* [36], the square root scaling is clearly inferior to the linear scaling, with R^2 values as low as 0.82 for the former, and values of 0.96 or above for the latter. Thus, data fitting gives no reason to prefer the square-root scaling law over a linear one for any of the datasets, and in some cases, the square root fit is not favored. It should also be pointed out that recent coarse-grained molecular simulations that contain electrostatic interactions between polyions and small ions but use only soft, generic local interactions spherical polymer beads and ions, do not produce the time-salt superposition Andreev *et al.* [66]. This suggests that local interactions are critical to an understanding of time-salt shifting, and we should not expect simple arguments based on the far-field Debye–Hückel analysis to be of much use.

Some of these considerations have led the Schlenoff group to discard relating the time-salt shift factor to dilute electrostatics governed by the Debye length. Instead, they start with a fundamental frequency of hopping, related to the rate ν_T at which ion pairs break. If this is enabled by a salt ion displacing a like-charged monomer from a monomer of opposite sign, then ν_T will be related to the salt ion diffusivity $D_{i,PEC}$ in the coacervate via

$$D_{i,PEC} = \frac{\nu_T d^2}{6}, \quad (8)$$

where d here is the hopping distance of the salt ion between sites along the PEs, which Akkaoui *et al.* take to be around 1 nm. (This distance is not the same as the distance d used in Eq. (5), although both are of order 1 nm or so.) From a measurement of the salt diffusivity in the coacervate, a value of ν_T was inferred that ranged from 6×10^7 to 1.8×10^8 rad/s with increasing salt concentration. The activation energy of this diffusivity determined by measuring the temperature dependence of $D_{i,PEC}$, was around $E_a \approx 20$ kJ/mol, which was then related to the probability p of an un-bound charged site on the coacervate via $E_a = -RT \ln(p)$, giving $p \approx 2 \times 10^{-4}$. The time τ_p is taken to be the time for a single ion pair to be broken, either in the absence of small salt ions, or because a small salt ion displaces the oppositely charged monomer; see Fig. 23. Akkaoui *et al.* [43] report a time of around $\tau_p \approx 10$ ns based on dielectric spectroscopy, which is roughly equal to the inverse of the ion hopping rate, i.e., $1/\nu_T$. This time is a factor of $1/p$ larger than the breakage attempt time, which is in the picosecond range, and $p \approx 2 \times 10^{-4}$ is again the fraction of attempts that lead to breakage of the ion pair, which is taken equal to the probability that a charge site in the coacervate is not bound by salt ion or an oppositely charged monomer. The longer, rheological, time scales are then taken to be proportional to τ_p , and also depend on the number of charge groups f on the chain and on the volume fraction ϕ of PE in the coacervate, the distance d between charged monomers, and the number of Kuhn steps N_e

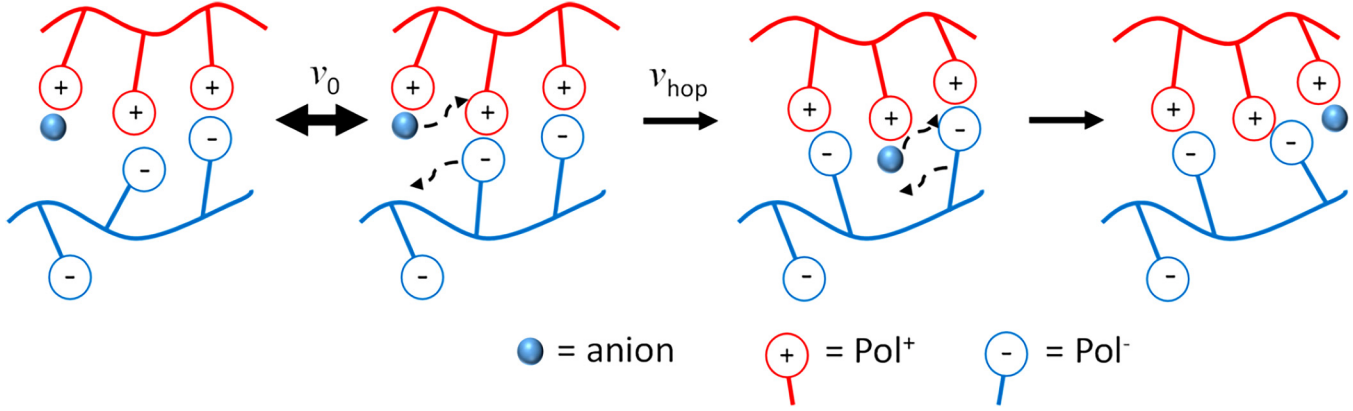


FIG. 23. Illustration of the displacement breakage of ion pairs by migration of a salt ion. Here, v_0 and v_{hop} are the attempted and actual hop frequency, where $v_{\text{hop}} = v_T$ [43]. Used with permission from Akkaoui *et al.*, *Macromolecules* **53**, 4234–4246 (2020). Copyright 2020, American Chemical Society.

in an entanglement segment. All of these factors can be dependent on salt concentration, and thus Akkaoui *et al.* interpret the salt dependence of the shift factor as a product of shift factors from each of these sources, $a_s = a_{s,\tau_p} a_{s,f} a_{s,\varphi} a_{s,d} a_{s,N_e}$; see Table II. This notional product of dependences does not yield any simple expression for the shift factor, such as $\ln a_s \propto -\sqrt{c_{\text{salt}}} + \text{const}$. However, as noted above, it is likely that the success of this square-root expression is fortuitous. If so, resolution of the source of the salt shift factor will require careful measurements of local dynamics using NMR or other sensitive experimental methods or use of molecular dynamics simulations. Table III gives formulas for rheological relaxation times adapted from the Rubinstein and Semenov [2] “sticky diffusion” model by the Schlenoff group [28] where the nomenclature was introduced in the above paragraphs, and l is the number of noncharged monomers between charged ones, with $l = 0$ if all monomers are charged; y is the “doping fraction,” or fraction of monomer charges that are bound by a small salt ion rather than by an oppositely charged monomer, and d is the distance between charged monomers. Relaxation times are reduced when ion pairs between polymers are diluted by bound small salt ions. N is the average number of Kuhn steps of PC and PA, assuming that they are similar and τ_b here is the effective or renormalized breakage time, which is the average time between ion-pair repairing events. This is presumably much longer than the time for ion-pair breaking, since most such broken ion pairs simply repair again rather than create ion-pairing with a different partner monomer.

Yang *et al.* [28] separated τ_b into two parallel relaxation channels, governed by constants $\tau_{b,i}$ and $\tau_{b,e}$ so that $\tau_b^{-1} = \tau_{b,i}^{-1} + \tau_{b,e}^{-1}$. Here, $\tau_{b,i}$ represents the “intrinsic” relaxation time for PE ion pairs Pol^+Pol^- , and was measured to be in the range $1.0\text{--}1.4 \times 10^{-4}$ s. $\tau_{b,e}$, which was reported to be of the order 10^{-7} s, reflects the “extrinsic” relaxation time for Pol^+A^- or Pol^+M^+ , where A^- and M^+ are a small salt anion and cation, respectively. As the salt doping level increases, $\tau_{b,e}$ dominates and determines the value of τ_b , thus decreasing the relaxation time for ionic bonds to form or break.

Following up with more recent work, the Schlenoff group [43] adapted entangled polymer theory to the PE “sticky reptation” model, giving time constants in Table IV. In this

table, τ_p is the ion-pair breakage time, f_e is the number of ion-pairs per entanglement segment, f is the total number of ion pairs in the chain, and τ_e is the “equilibration time,” or relaxation time of an entanglement segment. Note the power law N^5 for the chain-length dependence of reptation time τ_{rep} and zero-shear viscosity η_0 , suggested by Schlenoff and co-workers.

While the relationship between ion-pair “hopping frequency” and the overall rheology of coacervates as interpreted by sticky diffusion theory remains uncertain, the anomalies mentioned above call into question whether sticky diffusion really provides a complete picture of coacervate rheology. The anomalies that are particularly striking in the above discussion include (1) the asymmetry in changes in relaxation time produced by changing the molecular weight of PA versus PC, shown in Fig. 10; (2) the nonreptation power law of 5.4 in the dependence of viscosity on the degree of polymerization N in coacervates with nearly equal values of N for PC and PA in Fig. 9; and (3) the existence in a number of coacervates of a low-frequency plateau modulus, implying solidlike rather than liquidlike behavior at low frequency, in Figs. 13, 14, 19, and 20.

The first of these “anomalies” that of nonsymmetry in the effect of changing the molecular weight of PC versus PA could be explained by a difference in the hopping distance of oppositely charged monomers upon release of the ion pair. If, for example, the polycation monomer can, because of chain stiffness or other factors, move only a fraction of the distance that the polyanion can move before being bound to another ionic group, then the movement and relaxation of the

TABLE III. Formulas for relaxation times and viscosities adapted by Yang *et al.* from sticky diffusion theory.

	Rubinstein and Semenov [2]	Modification by Yang <i>et al.</i> [28]
Sticky Rouse	$\tau_R \sim \tau_b f^2$	$\tau_R \sim \tau_b N^2 (1-y)^2$
	$\eta_0 \sim \tau_b \left(\frac{k_B T}{d^2}\right) N l^{-2} \phi$	$\eta_0 \sim \tau_b \left(\frac{k_B T}{d^2}\right) N (1+l)^{-2} \phi$
Sticky reptation	$\tau_R \sim \tau_b f^2 \frac{N}{N_e}$	$\tau_R \sim \tau_b N^2 (1-y)^2 \frac{N}{N_e}$
	$\eta_0 \sim \tau_b \left(\frac{k_B T}{d^2}\right) \frac{N^3}{N_e} l^{-2} \phi$	$\eta_0 \sim \tau_b \left(\frac{k_B T}{d^2}\right) \frac{N^3}{N_e} (1+l)^{-2} \phi$

TABLE IV. Formulas for relaxation times and viscosities adapted by Akkaoui *et al.* from the reptation theory.

Reptation theory for nonsticky polymers	Modification for sticky polymers by Akkaoui <i>et al.</i> [43]
$\tau_e \sim \tau_o N_e^2$	$\tau_e \sim \tau_p f_e N_e^2 \sim \tau_p (1-y) N_e^3$
$\tau_{rep} \sim \tau_e \left(\frac{N}{N_e}\right)^3$	$\tau_{rep} \sim \tau_e \left(\frac{f}{N_e}\right)^2 \left(\frac{N}{N_e}\right)^3 \sim \tau_e (1-y)^2 \left(\frac{N}{N_e}\right)^5$
$\eta_0 \sim G_0 \tau_{rep} \sim \left[\frac{kT\phi}{d^3}\right] \tau_e \left(\frac{N}{N_e}\right)^3$	$\eta_0 \sim G_0 \tau_{rep} \sim \left[\frac{kT\phi}{d^3}\right] \tau_p (1-y)^3 \frac{N_e^5}{N_e^3}$

PC will be slower than the polyanion, even when the former has fewer monomers than the latter, and the chain length of the PC will have a greater effect on the relaxation time than that of the polyanion. Since the diffusivity of the monomer scales as the square of the hopping distance, a significant difference in their hopping distances could create a profound asymmetry in their effect on relaxation. We note in this respect that the polycation (PDMAEMA) has a Kuhn length of 2.65 nm in water, while for PAA, it is reported to be only 0.64 nm [22,33]. This suggests that the much greater rigidity of the PC may cause it to diffuse much less rapidly in response to loss of ion-pairing than does PAA, consistent with the experimental ion pairing. Whether this explanation is valid will require measurements of local hopping rates either by experiment or MD simulations. We note that the changes in PC chain length affect the rheology over the entire measured frequency range in Fig. 10(a), suggesting that the origin lies in short-range local interactions.

The second and third anomalies are likely not explainable by local motions alone, since their effects are primarily at the long-time scales, and do not show up in the high-frequency rheology. The second anomaly, that of the noncanonical 5.4 power law dependence of terminal relaxation time on molecular weight has been seen only once, and therefore awaits confirmation in some other system or by another lab. The third anomaly, the low-frequency plateau modulus, has been seen repeatedly and is evidently salt-concentration dependent. While the magnitude of low-frequency plateau is low enough in some cases to suggest that it might be a measurement artifact, in other cases it is easily large enough ($\sim 10^2$ to 10^4 Pa) to be unambiguously present. While not yet explained, there may be some inspiration to be drawn from neutral polymers with attractive interactions that leads them to form gels in some solvents, as occurs, for example, for isotactic polystyrene in nitropropane below the theta temperature [67]. A theory for such physical gelation has been developed by Tanaka and Stockmayer [68]. Application of these theories to coacervates has not yet been attempted, but may be a fruitful direction, with the caveat that successful application of such theories must, as a minimum, explain why some coacervates show the low-frequency plateau and others do not. Beyond qualitative success, much more detailed modeling will be required to see if these ideas have merit, and, if so, to make them quantitative and predictive.

XI. SUMMARY AND SUGGESTIONS FOR FUTURE WORK

Several thorough studies of coacervate rheology show the utility of the time-salt superposition in coacervate rheology

along with the conventional time-temperature superposition, and special systems, time-pH, and time-hydration superposition. The ability to shift linear rheology curves onto a master curve upon varying temperature, salt concentration, pH, and/or hydration suggests that these variables control local chain hopping rates but otherwise do not much affect larger-scale physics. Moreover, the similarity of the rheological curves to those for either unentangled solutions or entangled ones depending on chain length suggests a rather simple physical picture for coacervate rheology that deviates little from well-known behavior of neutral polymers at the coarse-grained level. Yet, there are several anomalies and exceptions to such a simple interpretation. Many coacervates show signs of a low-frequency gel-like plateau, whose presence and magnitude can depend on the salt concentration. When there is a terminal relaxation time, its scaling with chain lengths can deviate significantly from the conventional theory, and the separate dependencies of the terminal time on chain lengths of each of the two PEs, in the single case where they have been measured, show a strong asymmetry, thereby assigning an unequal role for polycation versus polyanion. The dependence of the “stickiness” lifetime of a temporary bond between PC and PA monomers is not well understood and seems to be highly system specific.

Thus, the linear rheology, not to speak of the nonlinear rheology, of PECs remains an intriguing topic for future research. Clear, detailed, and well-confirmed theories are not yet available, but common features in differing systems suggest that some broadly applicable theoretical concepts are ripe for discovery and exploitation. Beyond imaginative theorizing, definitive results will likely require more careful rheological experiments to establish the range of validity of the various superposition principles, to establish more clearly which PE systems have a low-frequency plateau modulus that is outside the range of experimental uncertainty, and to explore more widely the effects of different monomer and salt types. In addition, insightful experiments that probe local dynamics, such as advanced versions of NMR and neutron scattering, as well as accurate atomistic molecular dynamics simulations, should help resolve if and when local dynamics can be regarded as a kind of sticky diffusion governed by the breakage of ion pairs versus cooperative “glassy” dynamics involving multiple monomers and salt ions. High-quality PEs synthesized in nearly monodisperse form over a range of molecular lengths and studied over a range of temperatures, salt concentrations, and salt types will also be an essential part of bringing this important field to maturity over the next decade or two.

ACKNOWLEDGMENTS

The authors are grateful to the National Science Foundation (NSF) for supporting this research under Grant No. DMR 1707640. Any opinions, findings, and conclusions or recommendations expressed in this material are those of the authors and do not necessarily reflect the views of NSF.

REFERENCES

- [1] Liu, Y., H. H. Winter, and S. L. Perry, “Linear viscoelasticity of complex coacervates,” *Adv. Coll. Interf. Sci. Matter* **239**, 46–60 (2017).

- [2] Rubinstein, M., and A. N. Semenov, "Dynamics of entangled solutions of associating polymers," *Macromolecules* **34**, 1058–1068 (2001).
- [3] Meng, S., J. M. Ting, H. Wu, and M. V. Tirrell, "Solid-to-liquid phase transition in polyelectrolyte complexes," *Macromolecules* **53**, 7944–7953 (2020).
- [4] Sing, C. E., and S. L. Perry, "Recent progress in the science of complex coacervation," *Soft Matter* **16**, 2885–2914 (2020).
- [5] Rubinstein, M., Q. Liao, and S. Panyukov, "Structure of liquid coacervates formed by oppositely charged polyelectrolytes," *Macromolecules* **51**, 9572–9588 (2018).
- [6] Perry, S. L., and C. E. Sing, "Prism-based theory of complex coacervation: Excluded volume versus chain correlation," *Macromolecules* **48**, 5040–5053 (2015).
- [7] Zhang, P., K. Shen, N. M. Alsaifi, and Z. G. Wang, "Salt partitioning in complex coacervation of symmetric polyelectrolytes," *Macromolecules* **51**, 5586–5593 (2018).
- [8] Zhang, R., and B. I. Shklovskii, "Phase diagram of solution of oppositely charged polyelectrolytes," *Phys. A* **352**, 216–238 (2005).
- [9] de La Cruz, M. O., L. Belloni, M. Delsanti, J. P. Dalbiez, O. Spalla, and M. Drifford, "Precipitation of highly charged polyelectrolyte solutions in the presence of multivalent salts," *J. Chem. Phys.* **103**, 5781–5791 (1995).
- [10] Adhikari, S., M. A. Leaf, and M. Muthukumar, "Polyelectrolyte complex coacervation by electrostatic dipolar interactions," *J. Chem. Phys.* **149**, 163308 (2018).
- [11] Salehi, A., and R. G. Larson, "A molecular thermodynamic model of complexation in mixtures of oppositely charged polyelectrolytes with explicit account of charge association/dissociation," *Macromolecules* **49**, 9706–9719 (2016).
- [12] Friedowitz, S., A. Salehi, R. G. Larson, and J. Qin, "Role of electrostatic correlations in polyelectrolyte charge association," *J. Chem. Phys.* **149**, 163335 (2018).
- [13] Zhang, Y., F. Li, L. D. Valenzuela, M. Sammalkorpi, and J. L. Lutkenhaus, "Effect of water on the thermal transition observed in poly (allylamine hydrochloride)–poly (acrylic acid) complexes," *Macromolecules* **49**, 7563–7570 (2016).
- [14] Sing, C. E., "Micro- to macro-phase separation transition in sequence-defined coacervates," *J. Chem. Phys.* **152**, 024902 (2020).
- [15] Lin, Y., J. P. Brady, H. S. Chan, and K. Ghosh, "A unified analytical theory of heteropolymers for sequence-specific phase behaviors of polyelectrolytes and polyampholytes," *J. Chem. Phys.* **152**, 045102 (2020).
- [16] Danielsen, S. P. O., J. McCarty, J. Shea, K. T. Delaney, and G. H. Fredrickson, "Molecular design of self-coacervation phenomena in block polyampholytes," *Proc. Natl. Acad. Sci. U.S.A.* **116**, 8224–8232 (2019).
- [17] Spruijt, E., J. Sprakel, M. Lemmers, M. A. Cohen Stuart, and J. van der Gucht, "Relaxation dynamics at different time scales in electrostatic complexes: Time-salt superposition," *Phys. Rev. Lett.* **105**, 208301 (2010).
- [18] Spruijt, E., M. A. Cohen Stuart, and J. Van Der Gucht, "Linear viscoelasticity of polyelectrolyte complex coacervates," *Macromolecules* **46**, 1633–1641 (2013).
- [19] Ali, S., M. Bleuél, and V. M. Prabhu, "Lower critical solution temperature in polyelectrolyte complex coacervates," *ACS Macro Lett.* **8**, 289–293 (2019).
- [20] Wang, Y., V. Kozlovskaya, I. G. Arcibal, D. M. Crokek, and E. Kharlampieva, "Highly swellable ultrathin poly(4-vinylpyridine) multilayer hydrogels with pH-triggered surface wettability," *Soft Matter* **9**, 9420–9429 (2013).
- [21] Yoshida, M., "Solution properties of polyvinylpyridine in acid—II. Solution properties of poly(4-vinylpyridine) in aqueous solution of hydrochloric acid," *Eur. Polym. J.* **33**, 943–948 (1997).
- [22] Andreeva, L. N., S. V. Bushin, M. A. Bezrukova, T. N. Nekrasova, R. T. Imanbaev, V. D. Pautov, O. V. Nazarova, Y. I. Zolotova, and E. F. Panarin, "Conformation properties of poly(N, N-dimethylaminoethyl methacrylate) macromolecules in various solvents," *Russ. J. Appl. Chem.* **85**, 417–425 (2012).
- [23] Spruijt, E., F. A. M. Leermakers, R. Fokkink, R. Schweins, A. A. van Well, M. A. Cohen Stuart, and J. van der Gucht, "Structure and dynamics of polyelectrolyte complex coacervates studied by scattering of neutrons, X-rays, and light," *Macromolecules* **46**, 4596–4605 (2013).
- [24] Dickhaus, B. N., and R. Priefer, "Determination of polyelectrolyte pKa values using surface-to-air tension measurements," *Colloids Surf. A* **488**, 15–19 (2016).
- [25] Cranford, S. W., and M. J. Buehler, "Variation of weak polyelectrolyte persistence length through an electrostatic contour length," *Macromolecules* **45**, 8067–8082 (2012).
- [26] Mirtič, A., and J. Grdadolnik, "The structure of poly-L-lysine in different solvents," *Biophys. Chem.* **175**, 47–53 (2013).
- [27] Marciel, A. B., S. Srivastava, and M. V. Tirrell, "Structure and rheology of polyelectrolyte complex coacervates," *Soft Matter* **14**, 2454–2464 (2018).
- [28] Yang, M., J. Shi, and J. B. Schlenoff, "Control of dynamics in polyelectrolyte complexes by temperature and salt," *Macromolecules* **52**, 1930–1941 (2019).
- [29] Dautzenberg, H., E. Görnitz, and W. Jaeger, "Synthesis and characterization of poly(diallyldimethylammonium chloride) in a broad range of molecular weight," *Macromol. Chem. Phys.* **199**, 1561–1571 (1998).
- [30] Hirose, E., Y. Iwamoto, and T. Norisuye, "Chain stiffness and excluded-volume effects in sodium poly(styrenesulfonate) solutions at high ionic strength," *Macromolecules* **32**, 8629–8634 (1999).
- [31] Spiteri, M. N., F. Boué, A. Lapp, and J. P. Cotton, "Persistence length for a PSSNa polyon in semidilute solution as a function of the ionic strength," *Phys. Rev. Lett.* **77**, 5218 (1996).
- [32] Appel, P., and J. T. Yang, "Helix-coil transition of poly-L-glutamic acid and poly-L-lysine in D₂O," *Biochemistry* **4**, 1244–1249 (1965).
- [33] Li, H., B. Liu, X. Zhang, C. Gao, J. Shen, and G. Zou, "Single-molecule force spectroscopy on poly(acrylic acid) by AFM," *Langmuir* **15**, 2120–2124 (1999).
- [34] Taylor, T. J., and S. S. Stivala, "Small-angle X-ray scattering study of a weak polyelectrolyte in water," *J. Polym. Sci. B* **41**, 1263–1272 (2003).
- [35] Sauvage, E., D. A. Amos, B. Antalek, K. M. Schroeder, J. S. Tan, N. Plucktaveesak, and R. H. Colby, "Amphiphilic maleic acid-containing alternating copolymers—I. Dissociation behavior and compositions," *J. Polym. Sci. B* **42**, 3571–3583 (2004).
- [36] Hamad, F. G., Q. Chen, and R. H. Colby, "Linear viscoelasticity and swelling of polyelectrolyte complex coacervates," *Macromolecules* **51**, 5547–5555 (2018).
- [37] Ortiz, C., and G. Hadziioannou, "Entropic elasticity of single polymer chains of poly(methacrylic acid) measured by atomic force microscopy," *Macromolecules* **32**, 780–787 (1999).
- [38] Delaney, K. T., and G. H. Fredrickson, "Theory of polyelectrolyte complexation—Complex coacervates are self-coacervates," *J. Chem. Phys.* **146**, 224902 (2017).
- [39] Priftis, D., N. Laugel, and M. Tirrell, "Thermodynamic characterization of polypeptide complex coacervation," *Langmuir* **28**, 15947–15957 (2012).
- [40] Michaels, A. S., "Polyelectrolyte complexes," *Ind. Eng. Chem.* **57**, 32–40 (1965).
- [41] Markarian, M. Z., H. H. Hariri, A. Reisch, V. S. Urban, and J. B. Schlenoff, "A small-angle neutron scattering study of the equilibrium conformation of polyelectrolytes in stoichiometric saloplastic polyelectrolyte complexes," *Macromolecules* **45**, 1016–1024 (2012).

- [42] Fares, H. M., Y. E. Ghossoub, J. D. Delgado, J. Fu, V. S. Urban, and J. B. Schlenoff, "Scattering neutrons along the polyelectrolyte complex/coacervate continuum," *Macromolecules* **51**, 4945–4955 (2018).
- [43] Akkaoui, K., M. Yang, Z. A. Digby, and J. B. Schlenoff, "Ultraviscosity in entangled polyelectrolyte complexes and coacervates," *Macromolecules* **53**, 4234–4246 (2020).
- [44] Overbeek, J. T. G., and M. J. Voorn, "Phase separation in polyelectrolyte solutions. Theory of complex coacervation," *J. Cell. Comp. Physiol.* **49**, 7–26 (1957).
- [45] Lytle, T. K., and C. E. Sing, "Transfer matrix theory of polymer complex coacervation," *Soft Matter* **13**, 7001–7012 (2017).
- [46] Colby, J. D., *Viscoelastic Properties of Polymers*, 3rd Ed. (Wiley, New York, 1980).
- [47] Graessley W. W., *Polymeric Liquids and Networks Dynamics and Rheology* (Taylor & Francis Group, New York, 2008), p. 146.
- [48] Dealy, J. M., D. J. Read, and R. G. Larson, *Structure and Rheology of Molten Polymers: From Structure to Flow and Back Again*, 2nd Ed (Hanser, Cincinnati, 2018), pp. 265–266.
- [49] Colby, R. H., "Breakdown of time-temperature superposition in miscible polymer blends," *Polymer* **30**, 1275–1278 (1989).
- [50] Syed, V. M. S., and S. Srivastava, "Time-ionic strength superposition: A unified description of chain relaxation dynamics in polyelectrolyte complexes," *ACS Macro Lett.* **9**, 1067–1073 (2020).
- [51] Liu, Y., C. F. Santa Chalarca, R. N. Carmean, R. A. Olson, J. Madinya, B. S. Sumerlin, C. E. Sing, T. Emrick, and S. L. Perry, "Effect of polymer chemistry on the linear viscoelasticity of complex coacervates," *Macromolecules* **53**, 7851–7864 (2020).
- [52] Tekaat, M., D. Büttergerds, M. Schönhoff, A. Feryb, and C. Cramer, "Scaling properties of the shear modulus of polyelectrolyte complex coacervates: A time-pH superposition principle," *Phys. Chem. Chem. Phys.* **17**, 22552–22556 (2015).
- [53] Ikegami, A., and N. Imai, "Precipitation of polyelectrolytes by salts," *J. Polym. Sci.* **56**, 133–152 (1962).
- [54] Suarez-Martinez, P. C., P. Batys, M. Sammalkorpi, and J. L. Lutkenhaus, "Time-temperature and time-water superposition principles applied to poly (allylamine)/poly (acrylic acid) complexes," *Macromolecules* **52**, 3066–3074 (2019).
- [55] Zhang, Y., P. Batys, J. T. O'Neal, F. Li, M. Sammalkorpi, and J. L. Lutkenhaus, "Molecular origin of the glass transition in polyelectrolyte assemblies," *ACS Central Sci.* **4**, 638–644 (2018).
- [56] Zhang, R., Y. Zhang, H. S. Antila, J. L. Lutkenhaus, and M. Sammalkorpi, "Role of salt and water in the plasticization of PDAC/PSS polyelectrolyte assemblies," *J. Phys. Chem. B* **121**, 322–333 (2017).
- [57] Batys, P., Y. Zhang, J. L. Lutkenhaus, and M. Sammalkorpi, "Hydration and temperature response of water mobility in poly(diallyldimethylammonium)–poly (sodium 4-styrenesulfonate) complexes," *Macromolecules* **51**, 8268–8277 (2018).
- [58] Batys, P., S. Kivisto, S. M. Lalwani, J. L. Lutkenhaus, and M. Sammalkorpi, "Comparing water-mediated hydrogen-bonding in different polyelectrolyte complexes," *Soft Matter* **15**, 7823–7831 (2019).
- [59] Sadman, K., Q. Wang, Y. Chen, B. Keshavarz, A. Jiang, and K. R. Shull, "Influence of hydrophobicity on polyelectrolyte complexation," *Macromolecules* **50**, 9417–9426 (2017).
- [60] Huang, J., F. J. Morin, and J. E. Laaser, "Charge-density-dominated phase behavior and viscoelasticity of polyelectrolyte complex coacervates," *Macromolecules* **52**, 4957–4967 (2019).
- [61] Liu, Y., B. Momani, H. H. Winter, and S. L. Perry, "Rheological characterization of liquid-to-solid transitions in bulk polyelectrolyte complexes," *Soft Matter* **13**, 7332–7340 (2017).
- [62] Ali, S., and V. M. Prabhu, "Relaxation behavior by time-salt and time-temperature superpositions of polyelectrolyte complexes from coacervate to precipitate," *Gels* **4**(1), 11 (2018).
- [63] Shamoun, R. F., H. H. Hariri, R. A. Ghostine, and J. B. Schlenoff, "Thermal transformations in extruded saloplastic polyelectrolyte complexes," *Macromolecules* **45**, 9759–9767 (2012).
- [64] Ghostine, R. A., R. F. Shamoun, and J. B. Schlenoff, "Doping and diffusion in an extruded saloplastic polyelectrolyte complex," *Macromolecules* **46**, 4089–4094 (2013).
- [65] Ghasemi, M., S. Friedowitz, and R. G. Larson, "Analysis of partitioning of salt through doping of polyelectrolyte complex coacervates," *Macromolecules* **53**, 6928–6945 (2020).
- [66] Andreev, M., V. M. Prabhu, J. F. Douglas, M. Tirrell, and J. J. de Pablo, "Complex coacervation in polyelectrolytes from a coarse-grained model," *Macromolecules* **51**, 6717–6723 (2018).
- [67] Tan, H., A. Moet, A. Hiltner, and E. Baer, "Thermoreversible gelation of atactic polystyrene solutions," *Macromolecules* **16**, 28–34 (1983).
- [68] Tanaka, F., and W. H. Stockmayer, "Thermoreversible gelation with junctions of variable multiplicity," *Macromolecules* **27**, 3943–3954 (1994).
- [69] See supplementary material at <https://doi.org/10.1122/8.0000156> for (1) the comparison of all datasets discussed in Table II fitted by both square root and linear scaling rules using linear regression, and the goodness of fits, measured by the statistical values of R^2 ; (2) discussion of entanglement molecular weights inferred from plateau rheology; and (3) degree of polymerization, molecular weight, polydispersity index, and source of relevant polyelectrolytes mentioned in the Review.